Geochronology, 4, 577–600, 2022
https://doi.org/10.5194/gchron-4-577-2022

Constraining the geothermal parameters of in situ Rb–Sr dating on Proterozoic shales and their subsequent applications

Darwinaji Subarkah[1,2], Angus L. Nixon[3,2], Monica Jimenez[4], Alan S. Collins[1,2], Morgan L. Blades[1], Juraj Farkaš[5,2], Sarah E. Gilbert[6], Simon Holford[4], and Amber Jarrett[7]

[1]Tectonics & Earth Systems (TES), Department of Earth Sciences, University of Adelaide, Adelaide, SA 5005, Australia
[2]MinEx CRC, Australian Resources Research Centre, Perth, WA 6151, Australia
[3]Apatite Thermochronology Lab and Services (ATLaS), Department of Earth Sciences, University of Adelaide, Adelaide, SA 5005, Australia
[4]Stress, Structure and Seismic, Australian School of Petroleum and Energy Resources (ASPER), University of Adelaide, Adelaide, SA 5005, Australia
[5]Metal Isotope Group (MIG), Department of Earth Sciences, University of Adelaide, Adelaide, SA 5005, Australia
[6]Adelaide Microscopy, University of Adelaide, Adelaide, SA 5005, Australia
[7]Northern Territory Geological Survey, Darwin, NT 0801, Australia

Correspondence: Darwinaji Subarkah (darwinaji.subarkah@adelaide.edu.au)

Received: 7 March 2022 – Discussion started: 23 March 2022
Revised: 12 August 2022 – Accepted: 15 August 2022 – Published: 6 September 2022

Abstract. Recent developments in tandem laser ablation mass spectrometer technology have demonstrated the capacity for separating parent and daughter isotopes of the same mass online. As a result, beta-decay chronometers can now be applied to the geological archive in situ as opposed to through traditional whole-rock digestions. One novel application of this technique is the in situ Rb–Sr dating of Proterozoic shales that are dominated by authigenic clays such as illite. This method can provide a depositional window for shales by differentiating signatures of early diagenetic processes versus late-stage secondary alteration. However, the hydrothermal sensitivity of the Rb–Sr isotopic system across geological timescales in shale-hosted clay minerals is not well understood. As such, we dated the Mesoproterozoic Velkerri Formation from the Altree 2 well in the Beetaloo Sub-basin (greater McArthur Basin), northern Australia, using this approach. We then constrained the thermal history of these units using common hydrocarbon maturity indicators and modelled effects of contact heating due to the intrusion of the Derim Derim Dolerite.

In situ Rb–Sr dating of mature, oil-prone shales in the diagenetic zone from the Velkerri Formation yielded ages of 1448 ± 81, 1434 ± 19, and 1421 ± 139 Ma. These results agree with previous Re–Os dating of the unit and are interpreted as recording the timing of an early diagenetic event soon after deposition. Conversely, overmature, gas-prone shales in the anchizone sourced from deeper within the borehole were dated at 1322 ± 93 and 1336 ± 40 Ma. These ages are younger than the expected depositional window for the Velkerri Formation. Instead, they are consistent with the age of the Derim Derim Dolerite mafic intrusion intersected 800 m below the Velkerri Formation. Thermal modelling suggests that a single intrusion of 75 m thickness would have been capable of producing a significant hydrothermal perturbation radiating from the sill top. The intrusion width proposed by this model is consistent with similar Derim Derim Dolerite sill thicknesses found elsewhere in the McArthur Basin. The extent of the hydrothermal aureole induced by this intrusion coincides with the window in which kerogen from the Velkerri Formation becomes overmature. As a result, the mafic intrusion intersected here is interpreted to have caused kerogen in these shales to enter the gas window, induced fluids that mobilize trace elements, and reset the Rb–Sr chronometer. Consequently, we propose that the Rb–Sr chronometer in shales may be sensitive to temperatures of ca. 120 °C in hydrothermal reactions but can withstand temperatures of more than 190 °C in thermal systems not dominated by fluids. Importantly, this study demonstrates

a framework for the combined use of in situ Rb–Sr dating and kerogen maturation indicators to help reveal the thermochronological history of Proterozoic sedimentary basins. As such, this approach can be a powerful tool for identifying the hydrocarbon potential of source rocks in similar geological settings.

1 Introduction

The Rb–Sr isotopic system has historically been one of the most powerful dating tools in Earth science. Rb is abundant in K-rich minerals such as micas, clays, and K-feldspar, and these minerals are commonly found in a wide range of geological settings (Simmons, 1998). Therefore, it is an effective technique to date processes such as igneous emplacement, metamorphism, sedimentation, clay authigenesis, and hydrothermal alteration when these phases can be differentiated (Nebel, 2014). Its long half-life also makes it applicable to date events as early as the infant stages of our solar system (Nebel et al., 2011; Minster et al., 1979; Papanastassiou and Wasserburg, 1970). Traditionally, the application of this method required an arduous process of column chromatography to chemically separate the parent (^{87}Rb) and daughter (^{87}Sr) isotopes and avoid isobaric interference between the two elements (Hahn and Walling, 1938; Hahn et al., 1943; Charlier et al., 2006; Faure, 1977; Yang et al., 2010; Dickin, 2018). Alas, this approach has historically been expensive and time consuming and results in the loss of the genetic relationships between the minerals analysed, which has caused the technique to lose its popularity in recent years (Nebel, 2014).

Recent advancements in tandem laser ablation inductively coupled plasma mass spectrometry (LA-ICP-MS/MS) and similar instruments have revitalized the use of Rb–Sr by allowing them to be applied in situ (Zack and Hogmalm, 2016; Hogmalm et al., 2017; Bevan et al., 2021; Redaa et al., 2021a; Yim et al., 2021; Gorojovsky and Alard, 2020). Reactive gases such as N_2O and SF_6 can be introduced into a reaction cell between quadrupoles in an LA-ICP-MS/MS system, which permits the online separation of ^{87}Sr from ^{87}Rb through the measurement of the mass-shifted Sr reaction product (Zack and Hogmalm, 2016; Redaa et al., 2021a; Hogmalm et al., 2017). This allows for a more rapid and economic analysis time, as well as the ability to preserve petrographic relationships during these analyses. Consequently, secondary input of Rb or Sr from inclusions, zonation, alteration, and detritus can be isolated, resulting in a better understanding of the geochronological results. However, it should be noted that nanometre- or micrometre-sized mineral intergrowths of different origins still provide challenges when large spot sizes are used. The application of similar setups with other beta-decay dating systems have also yielded promising results (Tamblyn et al., 2021; Simpson et al., 2021; Ribeiro et al., 2021; Harrison et al., 2010; Hogmalm et al., 2019; Brown et al., 2022; Simpson et al., 2022; Scheiblhofer et al., 2022; Rösel and Zack, 2022; Gorojovsky and Alard, 2020; Bevan et al., 2021).

Hence, the in situ Rb–Sr dating method can now be used very similarly to laser ablation U–Pb dating, where age information can be obtained reliably, rapidly, and cheaply. In addition, the initial ^{87}Sr / ^{86}Sr ratio from the calculated isochron and the elemental data concurrently collected with the Rb and Sr isotopes can fingerprint the geochemical nature of the samples analysed (Subarkah et al., 2021; Redaa et al., 2021b; Tamblyn et al., 2020; Li et al., 2020). This approach has been shown to be capable of dating paragenetic sequences in deformation structures (Armistead et al., 2020; Tillberg et al., 2020), hydrothermal alteration assemblages (Laureijs et al., 2021), magmatic and metamorphic events (Li et al., 2020; Tamblyn et al., 2020), and metallogenic systems (Redaa et al., 2021b; Olierook et al., 2020; Şengün et al., 2019), whilst still preserving their micro-scale textural context.

Another novel use of this technique is to date Proterozoic shales in order to constrain their depositional window (Subarkah et al., 2021). Evidence suggests that clay minerals in Proterozoic shales are dominated by authigenic products from reverse weathering processes during reactions in equilibrium with the formation waters (Rafiei and Kennedy, 2019; Rafiei et al., 2020; Isson and Planavsky, 2018; Mackenzie and Kump, 1995; Kennedy et al., 2006; Deepak et al., 2022). Conversely, clay assemblages in late Ediacaran and Phanerozoic shales are commonly dominated by detrital products from continental weathering and erosion of soils and unstable parent rocks (Baldermann et al., 2020; Galán, 2006; Singer, 1980; Rafiei et al., 2020; Chamley, 1989; Hillier, 1995; Wilson, 1999; Kennedy et al., 2006). Simple multicellular organisms such as fungi and lichen have been shown to dramatically influence the rate of chemical weathering in continental rocks (Kennedy et al., 2006; Rafiei et al., 2020; Mergelov et al., 2018; Lee and Parsons, 1999; Cuadros, 2017; McMahon and Davies, 2018; Chen et al., 2000). As such, the surge in abundance of detrital clays in shales in the Ediacaran and Phanerozoic has been attributed to the production of soils driven by emergence of these microorganisms (Kennedy et al., 2006; Rafiei and Kennedy, 2019; Mergelov et al., 2018; Lee and Parsons, 1999; Zambell et al., 2012; McMahon and Davies, 2018). Thus, the primarily authigenic nature of clay minerals in Proterozoic shales makes them ideal targets for in situ Rb–Sr dating (Subarkah et al., 2021).

Despite the promising potential of the Rb–Sr isotopic system, the chronometer still holds some limitations. Rb and Sr are large ion lithophile elements that can sit in well-bound interstitial sites within a mineral lattice and be adsorbed onto the surface where they are more susceptible to fluid mobilization (Nebel, 2014; Villa, 1998; Li et al., 2019). In these environments, fluid-induced recrystallization and alteration can drive element and isotopic exchange at lower effective closure temperatures than those empirically determined for

classic thermal volume diffusion reactions (Dodson, 1973; Field and Råheim, 1979; Jenkin et al., 1995; Villa, 1998). Nevertheless, these complications can in turn be used advantageously to date secondary events such as episodes of hydrothermal fluid flow (Dodson, 1973; Shepherd and Darbyshire, 1981; Tamblyn et al., 2020; Li et al., 2020; Subarkah et al., 2021; Redaa et al., 2021b). However, it should be noted that the Rb–Sr system in shale-hosted illite may also be affected during diagenesis via the transformation of smectite to illite–smectite mixed-layer minerals.

In this study, we dated the Mesoproterozoic Velkerri Formation from the Roper Group of the McArthur Basin in northern Australia using in situ Rb–Sr geochronology and show that clay-mineral recrystallization in these shales occur at similar temperatures to kerogen catagenesis. The Roper Group is a good case study for in situ Rb–Sr shale dating, as it has been shown to be dominated by authigenic clays (Rafiei and Kennedy, 2019; Subarkah et al., 2021) and is chronologically well constrained (Ahmad and Munson, 2013; Kendall et al., 2009; Southgate et al., 2000; Bodorkos et al., 2022; Yang et al., 2020; Subarkah et al., 2021; Cox et al., 2022). Furthermore, the resurgence of interest in the resource potential of the organic-rich Velkerri Formation has also yielded a framework of palaeotemperature data that aim to discern the maturation history of hydrocarbons within the unit (Ahmad and Munson, 2013; Cox et al., 2016; George and Ahmed, 2002; Jarrett et al., 2019; Crick et al., 1988; Taylor et al., 1994; Summons et al., 1994; Volk et al., 2005; Lemiux, 2011; Revie, 2014; Capogreco, 2017).

Here, we targeted the Velkerri Formation (Fig. 1) from the thoroughly investigated well Altree 2 (Cox et al., 2016; NTGS, 1989; Lemiux, 2011; Revie, 2014; George and Ahmed, 2002; Jarrett et al., 2019; Nguyen et al., 2019; Nixon et al., 2021; Sander et al., 2018; NTGS, 2009, 2010, 2012; Yang et al., 2018; Capogreco, 2017; Cox et al., 2022). We show that common hydrocarbon maturation proxies such as T_{max} data from Rock-Eval pyrolysis, aromatic hydrocarbons, bitumen reflectance, and illite crystallinity can help define the temperature sensitivity of the Rb–Sr isotopic system in organic-rich shales. In addition, we have also modelled the geothermal aureole of a mafic intrusion that may have matured the kerogen into the gas window, altered trace elemental signatures, and reset the Rb–Sr isotopic system within the unit. As a result, we demonstrate that combining this novel dating method with traditional kerogen maturation proxies can be a powerful tool for reconstructing the thermochronological evolution of Proterozoic basin systems. This approach can then be applied to aid in hydrocarbon exploration for similar settings.

2 Geological background

The Palaeoproterozoic-to-Mesoproterozoic greater McArthur Basin is an intra-cratonic sedimentary system exposed across 180 000 km^2 of northern Australia (Ahmad and Munson, 2013). The basin is sub-divided into five unconformity-bounded sedimentary packages characterized by similarities in age, lithology, and stratigraphic position (Rawlings, 1999; Jackson et al., 1999). The Roper Group is part of the Wilton Package, which is the youngest of these sub-divisions (Rawlings, 1999; Jackson et al., 1987, 1999; Munson, 2016). The thickness of the Roper Group varies from around 1 to 5 km across several different fault zones (Jackson et al., 1987; Abbott and Sweet, 2000; Rawlings, 1999; Ahmad and Munson, 2013; Abbott et al., 2001). The Beetaloo Sub-basin (Fig. 1) is interpreted to be the main depocentre of the sedimentary system and preserves the thickest Roper Group sequences (Plumb and Wellman, 1987; Ahmad and Munson, 2013; Jackson et al., 1987; Abbott and Sweet, 2000). Lithologically, the Roper Group comprises a series of coarsening-upward sequences dominated by marine mudstone and interbedded sandstone with minor successions of intraclastic limestone (Abbott and Sweet, 2000; Jackson et al., 1987; Yang et al., 2018; Munson, 2016). Records of water-column euxinia and redox stratification, as well as fluctuating salinity levels, suggest that the Roper Group formed in an intermittently restricted marine basin within an epicontinental setting similar to the modern Black Sea or Baltic Sea (Revie and MacDonald, 2017; Yang et al., 2018; Ahmad and Munson, 2013; Mukherjee and Large, 2016; Cox et al., 2016, 2022).

Age constraints of the Roper Group have been established through several geochronological methods (Page et al., 2000; Ahmad and Munson, 2013; Subarkah et al., 2021; Kendall et al., 2009; Yang et al., 2019, 2020, 2018; Jackson et al., 1999; Nixon et al., 2021; Southgate et al., 2000). The beginning of the group's genesis is bracketed by a SHRIMP U–Pb zircon study from a tuff within the unconformably underlying Nathan Group as well as minimum depositional age from an in situ Rb–Sr analysis in the lower Roper Group that yielded ages of 1589 ± 3 and 1577 ± 56 Ma, respectively (Subarkah et al., 2021; Page et al., 2000). The unconformity between the Roper Group and the immediately underlying Nathan Group is likely related to the Isan Orogeny ca. 1.58 Ga (Jackson et al., 1999; Ahmad and Munson, 2013). Absolute dating of the Roper Group has been obtained through two SHRIMP U–Pb zircon studies from tuff layers in the Mainoru Formation, resulting in ages of 1492 ± 4 and 1493 ± 4 Ma (Jackson et al., 1999; Southgate et al., 2000). On the other hand, the Kyalla Formation at the top of the Roper Group is constrained to being deposited between the U–Pb age of its youngest detrital zircon at 1313 ± 47 Ma (Yang et al., 2018) and the age of crosscutting Derim Derim Dolerite intrusions at 1313 ± 1, 1324 ± 4, and 1327.5 ± 0.6 Ma (Yang et al., 2020; Bodorkos et al., 2022).

Mature organic-rich shales from the Velkerri Formation have been dated by Re–Os analysis at 1417 ± 29 and 1361 ± 21 Ma (Kendall et al., 2009). These ages have been interpreted to be the depositional age of the formation. The

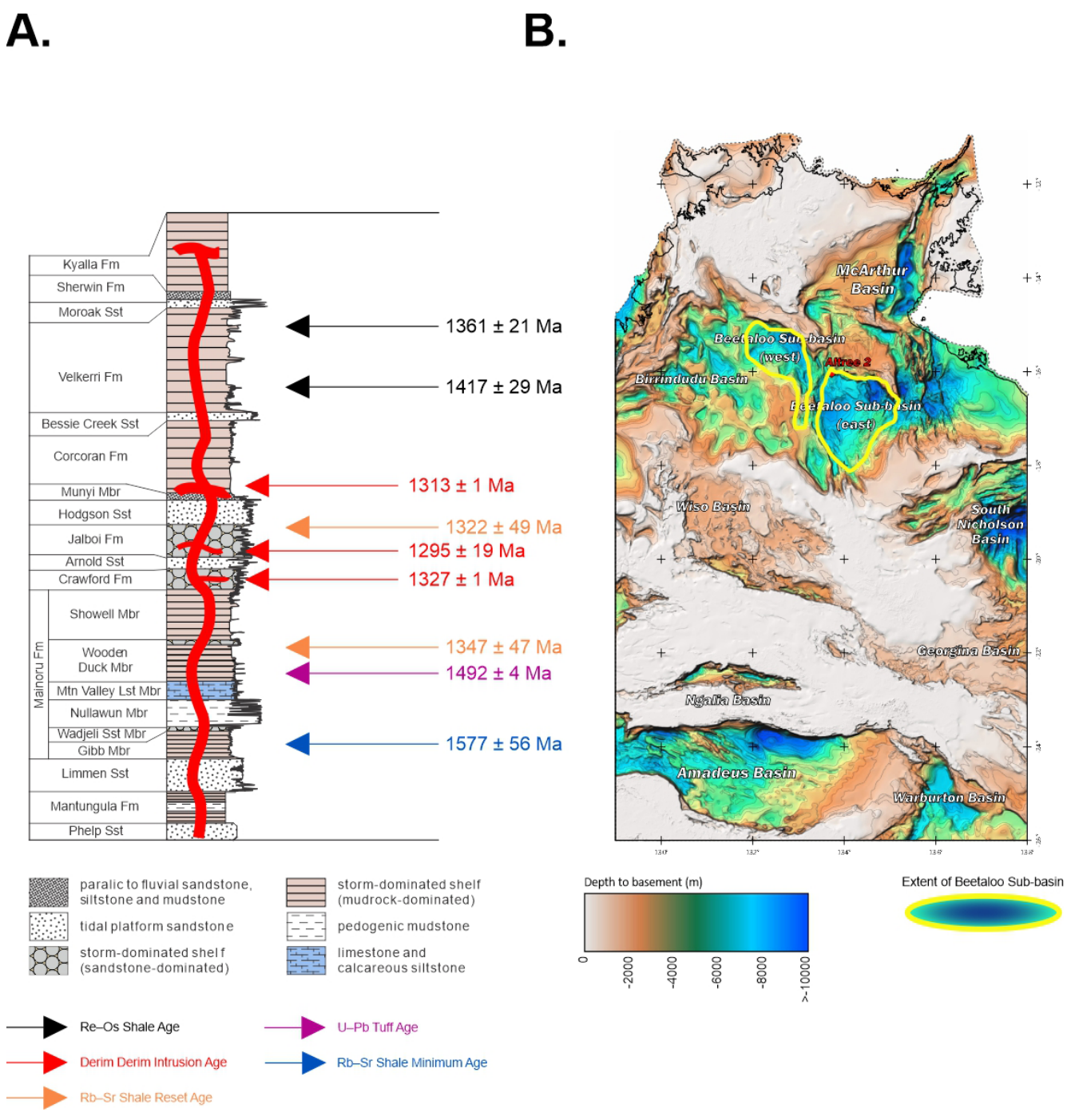

Figure 1. **(a)** Schematic stratigraphy and geochronological summary of the Roper Group (Abbott et al., 2001; Subarkah et al., 2021; Jackson et al., 1999; Southgate et al., 2000; Yang et al., 2020; Kendall et al., 2009). **(b)** Sample location and depth to basement map for the McArthur Basin, adapted from Frogtech Geoscience (2018).

geochronological constraints of the Roper Group are summarized in Fig. 1. The Velkerri Formation is dominated by deep-basinal lithologies such as mudstones and siltstones that coarsens upward into the cross-bedded Moroak Sandstone and Sherwin Ironstone (Abbott et al., 2001). The Velkerri Formation is interpreted to represent a deep-water, high-stand system tract within a marine environment (Abbott et al., 2001; Warren et al., 1998). The Velkerri Formation is commonly sub-divided into three distinct members (from bottom to top, the Kalala, Amungee, and Wyworrie members) based on variations in total organic carbon (TOC) content, gamma ray response, geochemistry, sedimentology, and

mineralogy (Munson and Revie, 2018; Cox et al., 2016, 2019; Warren et al., 1998; Revie, 2016; Ahmad and Munson, 2013; Jarrett et al., 2019).

Importantly, the McArthur Basin experienced a complex thermal history, following the deposition of the Roper Group, Mafic sills of the Derim Derim Dolerite widely intrude all units in the Roper Group at ca. 1330–1300 Ma, with the oldest intrusions likely contemporaneous with the end of sedimentation in the basin (Yang et al., 2020; Bodorkos et al., 2022; Nixon et al., 2021; Subarkah et al., 2021; Ahmad and Munson, 2013). Little evidence of subsequent tectonothermal perturbation is present within the basin until much of the region was overlain by subaerial basaltic lavas of the Kalkarindji Large Igneous Province (LIP) extruded at ca. 510 Ma (Evins et al., 2009; Glass and Phillips, 2006; Jourdan et al., 2014; Nixon et al., 2022). Following the Cambrian eruption of the Kalkarindji lavas, no significant ($> 110\,^{\circ}\mathrm{C}$) heating has been detected within the shallow parts of the basin (Duddy et al., 2004; Nixon et al., 2022).

The Altree 2 well drilled in the Beetaloo Sub-basin was chosen for this study as it intersects the entirety of the Velkerri Formation (Fig. 2). In addition, the well also intersected lavas of the Kalkarindji LIP directly overlying the Proterozoic sedimentary rocks and terminated at an intrusion of the Derim Derim Dolerite. Importantly, this well has also been the focus of numerous geochronological, geochemical, and geobiological investigations from academia, private explorers, and the Northern Territory Geological Survey (NTGS) that provide important complementary data to supplement this study (Cox et al., 2016, 2019; Jarrett et al., 2019; Yang et al., 2018; Nixon et al., 2021; Warren et al., 1998; George and Ahmed, 2002; Nguyen et al., 2019; Sander et al., 2018; Lemiux, 2011; NTGS, 2009, 2010, 2012; Bodorkos et al., 2022; Cox et al., 2022).

3 Methodology

Rock-Eval pyrolysis, aromatic hydrocarbon results, bitumen reflectance values, bulk x-ray diffraction (XRD) mineralogical compositions, and well log data were collated from several sources and compiled together in this study (NTGS, 1989, 2009, 2010, 2012; Cox et al., 2016; Lemiux, 2011; Revie, 2014; Capogreco, 2017; Revie et al., 2022; Jarrett et al., 2019). As such, their corresponding methodologies can be found in the references therein. The lithology of the Velkerri Formation was interpreted in detail (Fig. 2) using the electrical logs gamma ray (GR), neutron (NPRS), and density (RHOB) of the Altree-2 well (NTGS, 1989). Four lithologies were defined after applying cut-offs at each electrical log. They are then correlated along depth. Sandstone units corresponds to a GR < 130 API, NPRS < 0.20 %, and RHOB of around $2.5\,\mathrm{g\,cm^{-3}}$. This relates to a crossover between the RHOB and NPRS logs and competent material at the GR. Interbedded shale and sands are defined by a GR > 130 and < 250 API, NPRS > 0.20 and $< 0.25\,\mathrm{m^3\,m^{-3}}$, and RHOB between 2.5 and $2.53\,\mathrm{g\,cm^{-3}}$. This lithology reflected a smaller breach between the density and neutron logs in comparison to the previous sandstone lithology. Shale units were constrained by a GR > 250 API, NPRS $> 0.25\,\mathrm{m^3\,m^{-3}}$, and RHOB $> 2.53\,\mathrm{g\,cm^{-3}}$, with a minimum separation (or no separation) between the porosity logs. On the other hand, dolomitic siltstones have a GR response similar to the sandstone, with NPRS ranging between 0.25 to 0.27 and RHOB $> 2.62\,\mathrm{g\,cm^{-3}}$. This indicates a competent lithology in the GR with a gap between the neutron and density curves. In addition, $T_{\max}$ data were also collated to discriminate the hydrocarbon maturation levels downhole. From this, a shift in hydrocarbon potential and $T_{\max}$ gradients were identified at around 900 m (Fig. 2), where kerogen enters the gas window and becomes overmature. Five shale chips were then sampled from the Velkerri Formation in Altree 2 at depths of 415, 520, 696, 938, and 1220 m for further characterization.

Samples were first imaged for their mineral composition and petrographic relationships. Backscatter electron (BSE) imaging and mineral liberation analysis (MLA) maps of samples were collected using a Hitachi SU3800 automated mineralogy scanning electron microscope at Adelaide Microscopy. BSE image tiles were done at 10 mm working distance and 20 kV acceleration voltage with MLA maps completed using a raster analysis using spectra collected at 0.35 µm per pixel resolution. Minerals previously categorized by bulk XRD analysis of the Velkerri Formation from Cox et al. (2016) were used to develop a "library" to help identify phases found by spectral reflectance MLA mapping. In situ Rb–Sr geochronology and trace element analysis studies were undertaken at Adelaide Microscopy using a laser ablation (RESOlution-LR ArF 193 nm excimer laser) inductively coupled plasma tandem mass spectrometer (Agilent 8900x ICP-MS/MS) with analytical parameters and tuning conditions following Redaa et al. (2021a). The laser setup used in this study is provided in the Supplement. Laser ablation data and error correlations were processed using the LADR software package (Norris and Danyushevsky, 2018; Schmitz and Schoene, 2007). During the data-processing step, Zr, Si, Ti, and rare-earth element signatures were monitored to filter the detrital component of each analysis. Non-stable isotopic and elemental signatures were also culled or cropped during the processing of each analysis to aid in ensuring spot homogeneity. The $^{87}\mathrm{Rb}$ decay constant used was $0.000013972 \pm 4.5 \times 10^{-7}\,\mathrm{Myr^{-1}}$ following Villa et al. (2015). Isochron and single-spot ages were calculated with ISOPLOTR (Vermeesch, 2018). Single-spot ages were calculated using the isochron intercept as their initial $^{87}\mathrm{Sr}/^{86}\mathrm{Sr}$ ratios (Vermeesch, 2018; Nebel, 2014; Rösel and Zack, 2022). In addition, kernel density estimation (KDE) graphs (Vermeesch, 2012), cumulative age distribution (CAD) plots (Vermeesch, 2007), and multidimensional scaling (MDS) graphs (Vermeesch, 2013) were also

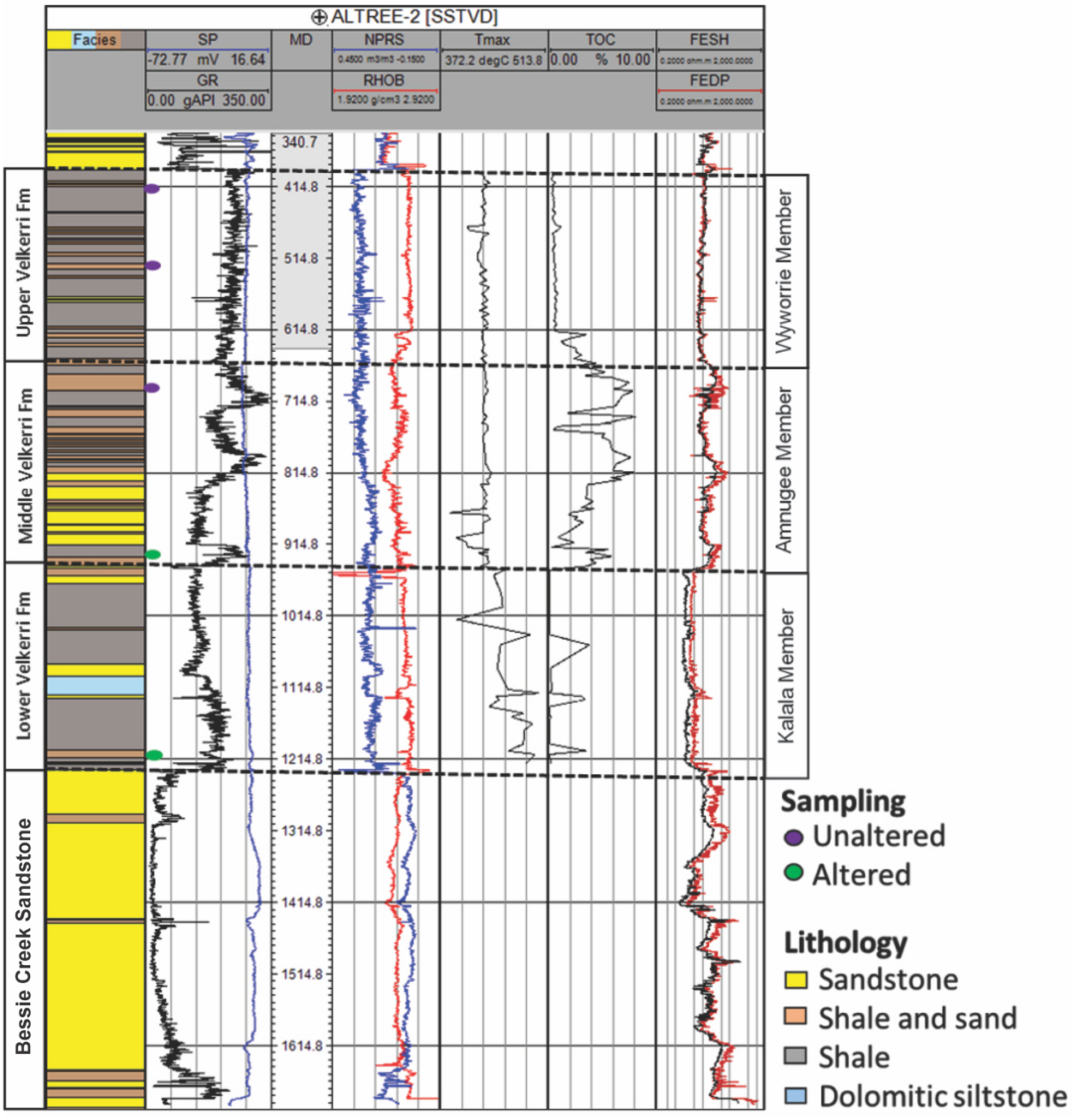

Figure 2. Summary of reprocessed downhole well log data for Altree 2.

constructed using ISOPLOTR (Vermeesch, 2018) to differentiate between the population of single-spot ages from each sample.

The phlogopite nano-powder Mica-Mg (Govindaraju et al., 1994) was used as the primary reference material, and its natural mineral equivalent, MDC from the Ampandrandava Mine in Madagascar (Hogmalm et al., 2017; Armistead et al., 2020; Redaa et al., 2021a; Li et al., 2020), and glauconite grain reference material GL-O (Derkowski et al., 2009; Charbit et al., 1998) were used secondary age standards. As previously discussed in Subarkah et al. (2021), nano-powdered reference materials have similar ablation characteristics to fine-grained shales, with analogous matrix effects. As such, they are ideal standards for in situ analyses of these samples.

When anchored to a $^{87}Sr/^{86}Sr$ initial ratio of 0.72607 ± 0.00363 as reported by Hogmalm et al. (2017), MDC yielded an age of 524 ± 7 Ma. This is within the error of the published mean age of Mica-Mg at 519 ± 7 Ma (Hogmalm et al., 2017). In addition, the independent reference material GL-O gave an age of 96 ± 4 Ma, accurate

to its published K–Ar age of 95 ± 1.5 Ma (Charbit et al., 1998; Derkowski et al., 2009). It should be noted that this age is younger than the tuff-horizon age of the GL-O host rock, dated at 113 ± 0.3 Ma (Selby, 2009). Consequently, the ages yielded from GL-O have instead been proposed to be indicative of the formation of glauconite occurring early after the deposition of the host rock (Selby, 2009).

Glass standard NIST SRM 610 was used as a primary standard for elemental quantification in this study. Analysis of secondary standard BCR-2G yielded a combined major, trace, and rare-earth element composition that was in good agreement (Pearson $R > 0.999$, Pearson $R^2 > 0.999$, and p Value < 0.0001) with their published values as compiled in the GeoREM database (Jochum et al., 2005; Pearce et al., 1997; Jochum et al., 2011; Jochum and Stoll, 2008).

One-dimensional thermal modelling of the Altree 2 well was conducted using the SILLi 1.0 numerical model, which is designed for simulating thermal perturbation associated with sill emplacement within sedimentary basins (Iyer et al., 2018). First, palaeotemperatures were estimated from the compiled thermal maturity data (Disnar, 1994, 1986; Waliczek et al., 2021) following equations based on similar sedimentary systems that experienced a heating event due to burial and a subsequent igneous intrusion (Piedad-Sánchez et al., 2004). Forward modelling was then conducted to replicate maximum thermal conditions calculated in the well from the thermal maturity data, where palaeotemperatures suggest that the Wyworrie and Amungee members experienced significant additional sedimentary cover in the Mesoproterozoic. During modelling, an additional 1.5 km of sedimentary rocks were added above the erosional unconformity now present above the McArthur Basin fill (Hall et al., 2021), while all post-Mesoproterozoic units were excluded. The upper contact of a sill with an initial temperature of 1150 °C (Wang et al., 2012) was set at 2868 m, in accordance with adjusted burial depths during the Mesoproterozoic. As sill thickness is unconstrained within the Altree 2 well, multiple iterations were run with different thicknesses in order to establish the scenario able to best satisfy the thermal aureole extent observed in this well. From this, a sill thickness of 75 m was considered most appropriate and is consistent with Derim Derim sill thicknesses of $\sim$ 10–100 m commonly observed across the basin (Lanigan and Torkington, 1991; Lanigan and Ledlie, 1990; Ledlie and Maim, 1989; NTGS, 2014, 2015, 2016). Full modelling parameters and petrophysical properties are provided in Tables S2 and S3 in the Supplement.

4 Results

4.1 Compilation of legacy data

All legacy data are compiled in the Supplement and were checked for quality before interpretation, as several factors, such as contamination of cuttings due to drilling fluid or poor organic content, can make results unreliable (Carvajal-Ortiz and Gentzis, 2015; Dembicki, 2009; Peters, 1986). Rock-Eval pyrolysis values were screened using the thresholds described by Hall et al. (2016). Data were subsequently excluded from interpretation if these criteria were not met. More than 90 % of the data yielded S2 > 0.1 mg HC g^{-1}, indicating that they were sufficiently abundant in organic content to provide well-defined peaks for characterizing T_{max} and hydrogen index. Importantly, compilation of Rock-Eval pyrolysis values were all internally consistent (e.g. hydrogen index that is equal to S2 / TOC $\times$ 100). Next, there was no evidence of anomalously low T_{max} values (< 380 °C) present. Extremely low T_{max} values are commonly a product of incorrect selection of the S2 peak by the programme or the widening of the S1 peak from non-indigenous free hydrocarbons. T_{max} results compiled in this study range between 384 and 502 °C with a mean of 433 °C (SD = 17). TOC content in the Velkerri Formation varies from 0.07 % to 8.07 %, averaging 2.25 % (SD = 2.26). Clay mineral crystallinity and size data sourced for this compilation were standardized for interlaboratory comparisons (Warr and Rice, 1994; Warr and Mählmann, 2015). Full width at half maximum values from Altree 2 shale samples were computationally remeasured as a secondary check (Capogreco, 2017; NTGS, 2010, 2012). A total of 13 samples from the Velkerri Formation were analysed for their illite crystallinity. The Kübler index for these shales range between 0.88 to 0.36, with decreasing values at depth and the lowest data originating from the Kalala Member. The methylphenanthrene distribution factor (MPDF), methylphenanthrene ratios (MPR), and bitumen reflectance data collated from Jarrett et al. (2019) and Revie et al. (2022) also display an increasing trend downhole.

4.2 Mineralogy of the Velkerri Formation

A total of 11 mineral phases were identified by bulk XRD analysis of the Velkerri Formation from Cox et al. (2016). The major mineral phases were quartz, kaolinite, illite, and orthoclase, which on average make up 90 % of the total composition of the samples. Trace minerals include glauconite, montmorillonite, pyrite, magnetite, siderite, dolomite, and plagioclase. Our MLA mapping also identified these assemblages. Importantly, the two different methods categorized these minerals at similar abundances. However, results from MLA mapping also found other mineral assemblages not identified by bulk XRD analysis, including biotite, chlorite, clinochlore, apatite, and zircon. These differences could be due to the slightly different sub-intervals from which samples were analysed. Bulk XRD is a destructive procedure, and therefore the same section cannot be reused for in situ analysis. As a result, samples spaced 1–2 cm apart may yield different results. In addition, the targeted areas for MLA are often spatially localized and only based on 2D information. As such, they may not be representative for the bulk rock, making the comparison with XRD datasets difficult. The com-

plete mineralogical abundance and correlations between the results of bulk XRD analysis and MLA mapping are summarized in Table 1. Extensive petrographic descriptions of all samples can be found in the Supplement.

4.3 Laser ablation data

Geochronological results yielded by samples from the Wyworrie and Amungee members gave ages within error of each other. The sample from 415 m depth was dated at 1448 ± 81 Ma. Next, the mudstone analysed from 520 m depth yielded an age of 1434 ± 19 Ma. Thirdly, the shale sample studied from 696 m depth resulted in an age of 1411 ± 139 Ma. A Kalala Member shale chip from 938 m at depth was dated at 1322 ± 93 Ma. Another sample from this member, towards the boundary with the underlying Bessie Creek Sandstone at depth 1220 m resulted in an age of 1336 ± 40 Ma. The range of precision from these Rb–Sr ages is primarily constrained by a substantial spread in $^{87}Rb / ^{86}Sr$ ratios, the number of data points defining the regression line, and errors in each individual analysis (Nebel, 2014). The most precisely dated samples, extracted from 520 and 1220 m depth, had the widest range of $^{87}Rb / ^{86}Sr$ ratios (0–50), whilst the other two samples preserved a range of $^{87}Rb / ^{86}Sr$ values less than 10 (Fig. 6). The variability in these values could be a subject of future studies in order to improve the success of this dating method. Single-spot ages were calculated for all spot analyses in each sample, and their populations categorically differ (Fig. 8).

Elemental concentrations of each sample were concurrently collected during the in situ Rb–Sr laser ablation investigation, and they are in good agreement with data collected by bulk geochemical analysis from Cox et al. (2016). Samples from depths of 415, 520, and 696 m do not show any covariation between their total rare-earth elements and yttrium (REEY) concentrations and Sm / Nd ratios (Fig. 7). On the other hand, the sample from 938 m showed a statistically significant relationship between these two parameters (Pearson $R = 0.58$; Pearson $R^2 = 0.336$; p value < 0.0001). In addition, Velkerri Formation shale sourced from 1220 m depth also showed a strong covariation between total REEY values and Sm / Nd (Pearson $R = -0.545$; Pearson $R^2 = 0.297$; p value < 0.0001). These associations were also identified in the whole-rock geochemical data collected from Cox et al. (2016). Figure 7b shows that samples between 390 and 900 m depth hold no statistically significant relationships between the two factors. However, samples from deeper than 900 m display a strong relationship between the two variables (Pearson $R = -0.559$; Pearson $R^2 = 0.312$; p value $= 0.003$). The full geochronological and inorganic geochemical dataset for samples in this study can be found in the Supplement.

4.4 Thermal modelling

One-dimensional thermal modelling of the emplacement of a 75 m thick Derim Derim Dolerite sill at the base of the Altree 2 well is sufficient to produce a thermal aureole reaching temperatures $> 110\,^{\circ}C$, ca. 800 m above the top contact of the sill (Fig. 9a). Maximum palaeotemperatures recorded in the Wyworrie Member exceed those predicted in this simulation; however, this may be attributed to elevated temperatures in the shallow basin during eruption of the Kalkarindji LIP in the Cambrian (Nixon et al., 2022). The resultant maximum thermal profile is consistent with palaeotemperature estimates derived from T_{max} and is thus considered a plausible model for the observed data from the well. Post-intrusion temperatures at depths that match the samples with reset Rb–Sr ages are much lower than observed in comparable isotopic systems for thermally induced diffusion (Dodson, 1973; Tillberg et al., 2020; Torgersen et al., 2015; Yoder and Eugster, 1955), with the shallowest reset sample peaking at ca. $120\,^{\circ}C$. Furthermore, elevated temperatures predicted by the modelling are geologically short lived, with temperatures returning to steady-state conditions by approximately half a million years after sill intrusion (Fig. 9b).

5 Thermal maturity of the Velkerri Formation

Geochemical and mineralogical-based thermal maturity indicators collected via Rock-Eval studies and bulk XRD analyses were compiled in this study in order to establish a vertical profile of the Velkerri Formation and assess the local palaeo-thermal structure. The T_{max} parameter is the temperature at which the maximum rate of hydrocarbon generation occurs during pyrolysis analysis and is a common method used to reconstruct thermal histories of basin systems (Espitalié, 1986; Espitalié et al., 1977; Peters and Cassa, 1994; Welte and Tissot, 1984). Additionally, the Kübler index (KI) is determined by the XRD reflection of illite and is also a popular maturation proxy used to classify low-grade metamorphism in pelitic rocks (Kubler, 1967; Guggenheim et al., 2002; Blenkinsop, 1988). However, both of these thermal indicators can be influenced by multiple factors other than burial-related heating, and they therefore struggle to resolve absolute quantitative palaeotemperatures. Changes in heating rate; abundance in hydrogen, sulfur, and uranium content; or the organic richness of samples can result in inaccurate T_{max} values (Yang and Horsfield, 2020; Peters, 1986; Dembicki, 2009; Espitalié et al., 1977). Similarly, the KI has also been shown to be sensitive to several parameters, such as changes in heating rate and geochemical variability in the sample's initial mineralogy (Eberl and Velde, 1989; Warr and Mählmann, 2015; Abad and Nieto, 2007; Mählmann et al., 2012). In addition, variations in procedures between laboratories can further complicate the direct comparison of these values (Cornford et al., 1998; Jarvie, 1991; Peters and Cassa, 1994; Tissot et al., 1987). Consequently, these thermal indi-

Table 1. **(a)** Mineralogical abundance of the Velkerri Formation shales collected by bulk XRD analysis from Cox et al. (2016) and spectral reflectance MLA mapping in this study. All values are in weight percentage. **(b)** Covariation between the mineral phases categorized by both methods.

(a)

Depth	Method	Apatite	Biotite	Chlorite	Dolomite	Glauconite	Illite	Kaolinite	Magnetite	Montmorillonite	Orthoclase	Pyrite	Quartz	Siderite	Zircon	Plagioclase
415 m	Bulk XRD	0.00	0.00	0.00	0.25	0.82	34.05	21.25	0.36	1.79	13.33	0.28	26.13	1.76	0.00	0.00
	MLA map	0.00	1.22	1.33	0.00	0.00	35.52	7.45	0.89	9.05	11.48	0.40	23.93	0.00	0.02	4.39
520 m	Bulk XRD	0.00	0.00	0.00	0.37	2.35	43.28	17.14	0.38	2.01	10.01	0.74	23.67	0.05	0.00	0.00
	MLA map	0.00	0.07	0.08	0.00	0.00	36.51	7.11	0.00	0.04	4.08	0.24	47.94	0.00	0.00	0.85
696 m	Bulk XRD	0.00	0.00	0.00	0.21	1.53	27.59	2.07	0.00	1.49	13.40	4.11	45.02	0.00	0.00	4.57
	MLA map	0.31	0.93	0.06	0.00	0.00	18.48	0.00	0.00	4.00	8.27	4.47	60.88	0.00	0.00	1.41
938 m	Bulk XRD	0.00	0.00	0.00	0.53	1.36	27.03	6.99	0.33	1.16	11.32	1.49	43.28	0.01	0.00	6.50
	MLA map	1.2	0.00	0.06	0.00	0.00	22.13	5.46	0.00	0.00	3.37	1.60	57.79	0.00	0.00	6.90
1220 m	Bulk XRD	0.00	0.00	0.00	0.43	1.04	39.36	13.99	0.42	1.66	7.32	0.26	33.56	0.10	0.00	1.86
	MLA map	0.00	0.01	0.01	0.05	0.00	38.18	20.21	0.00	0.00	4.45	0.01	35.25	0.00	0.01	1.63

(b)

Depth (m)	Pearson R	Pearson R 95 % C.I.	Pearson R^2	p value
415	0.922	0.784–0.973	0.850	< 0.0001
520	0.866	0.648–0.953	0.750	< 0.0001
696	0.953	0.868–0.984	0.910	< 0.0001
938	0.965	0.898–0.988	0.930	< 0.0001
1220	0.989	0.969–0.996	0.979	< 0.0001

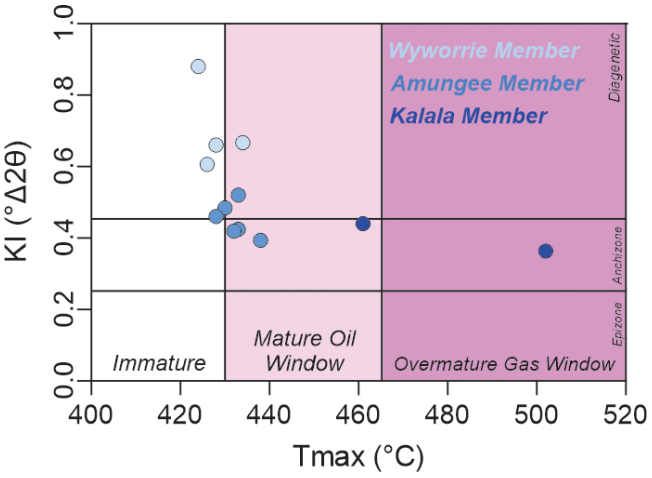

Figure 3. Covariation between T_{max} values from pyrolysis analysis and illite crystallinity KI in the Velkerri Formation. An increase in T_{max} coincides with a decrease in KI, suggesting that these proxies are both mainly sensitive to changes in palaeotemperature.

cators need to be treated with caution when applied independently and are more suitable as qualitative discriminators as opposed to absolute quantitative parameters. However, such proxies can be more confidently used to estimate palaeotemperatures in sedimentary successions if they show a strong relationship with each other (Dellisanti et al., 2010; Ola et al., 2018; Waliczek et al., 2021; Burtner and Warner, 1986; Velde and Espitalié, 1989). Ultimately, both organic and inorganic indicators are essential for a robust understanding of the thermal histories of sedimentary sequences through time.

In this study, we examine the covariation between the T_{max} values and KI to reconstruct the thermal history of the Velkerri Formation in the Altree 2 well (Fig. 3). In our compilation, samples with immature kerogen ($T_{max} < 435\,°C$) correspond to rocks in the diagenetic zone (KI $> 0.45°\ \Delta 2\theta$). This relationship is true in similar studies and generally translates to palaeotemperatures of ca. 100 °C (Dellisanti et al., 2010; Espitalié et al., 1977; Kosakowski et al., 1999; Kubler, 1967; Abad and Nieto, 2007).

Interestingly, the samples within the mature oil window ($435\,°C < T_{max} < 465\,°C$) show a wide range of KI values between 0.39 and $0.65°\ \Delta 2\theta$ (Fig. 3). This is possibly due to the delay between thermal reactions in clay minerals as opposed to organic matter (Ola et al., 2018). Although the maturation of organic matter and the morphology of clay minerals both largely depend on temperature, other processes such as the kinetics of the thermal reaction and geochemical composition of the sample can make these relationships non-linear (Ola et al., 2018; Velde and Vasseur, 1992; Pollastro, 1993; Varajao and Meunier, 1995; Meunier et al., 2004). The disparity between kerogen evolution and the equilibrium stage of illitization at these temperatures may also play a role in this variability (Dellisanti et al., 2010). Nevertheless, an increase in T_{max} pyrolysis results from these samples still appears to correlate with a decrease in KI values. These thermometers would approximately equate to palaeotemperatures between 100 and 150 °C (Merriman and Frey, 1999; Árkai et al., 2002; Kosakowski et al., 1999; Welte and Tissot, 1984).

On the other hand, the sample displaying overmature kerogen ($T_{max} > 465\,°C$) corresponds to the smallest KI value (Fig. 3) of $0.36°\ \Delta 2\theta$ (Dellisanti et al., 2010). These values commonly define the gas window and the anchizone, corresponding to palaeotemperatures of ca. 200 °C (Kosakowski et al., 1999; Árkai et al., 2002; Dellisanti et al., 2010). Overall, a trend between increasing T_{max} and decreasing KI values (Fig. 3) confirms the feasibility of these parameters as thermal maturation proxies (Dellisanti et al., 2010).

Lastly, the thermal parameters for the Velkerri Formation can be further examined by inspecting the changes in MPDF (Kvalheim et al., 1987; Boreham et al., 1988), MPR (Wilhelms et al., 1998; Radke et al., 1982), and bitumen reflectance (Riediger, 1993). Previous studies have shown that aromatic hydrocarbons were effective in providing thermal constraints for the Velkerri Formation (George and Ahmed, 2002; Jarrett et al., 2019). These proxies were similarly sensitive to maturity variations from the thermally immature window to late oil window. As such, we normalize the thermal indicators used in this study by converting them all (Jarvie et al., 2001; Revie et al., 2022; Jarrett et al., 2019) to calculated vitrinite reflectance values (VR_{CALC}; Fig. 4). The VR_{CALC} values from four different thermal indicators show that the Velkerri Formation quickly elevated in maturity and enters the gas window at ca. 900 m depths (Fig. 4). The agreement of all proxies add further confidence to the temperature constrains used in this study.

Multiple geochemical and mineralogical thermal parameters from our compiled dataset demonstrate strong correlation between them, suggesting that the proxies used in this study primarily recorded changes in palaeotemperature as opposed to other possible variables. Notably, five different, independent, source-rock maturation proxies statistically agree and recorded similar step-wise increases in thermal history downhole. As such, we investigated five samples approaching the geothermal anomaly in the Kalala Member for in situ Rb–Sr and trace element analysis. The changes in thermal maturation indexes throughout the well are used to help constrain the parameters of the Rb–Sr isotopic system in Proterozoic shales.

6 Thermochronological history of the Velkerri Formation

Although some of the geochronological results of these samples may overlap due to their errors (Fig. 6), they are still categorically different downhole (Fig. 8). We display these differences by plotting the population of single-spot ages from

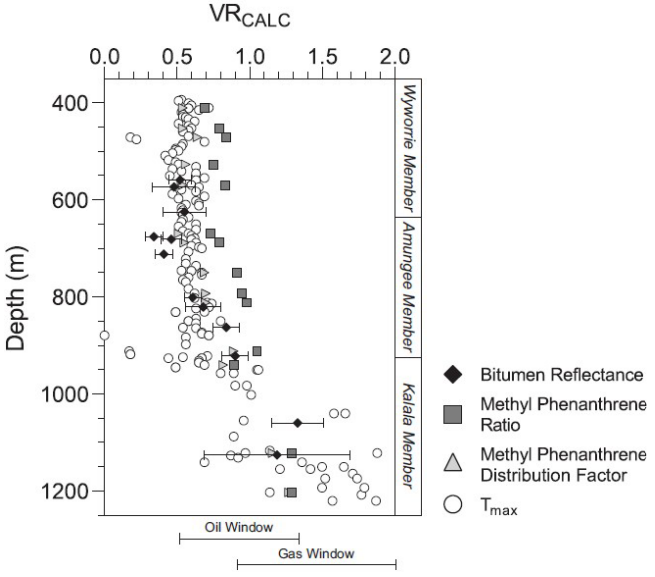

Figure 4. Calculated vitrinite reflectance (VR_{CALC}) data modelled downhole from T_{max}, MPR, MPDF, and bitumen reflectance data compiled in this study (NTGS, 1989, 2009, 2010, 2012; Cox et al., 2016; Lemiux, 2011; Revie, 2014; Capogreco, 2017; Revie et al., 2022; Jarrett et al., 2019). VR_{CALC} from all proxies indicate an elevation in thermal maturity into the gas window at depths ca. 900 m.

each sample against each other. Kernel distribution estimate (KDE) plots of these results show that the distribution of single-spot ages from samples shallower than 900 m largely overlaps with the Re–Os age constraint (Fig. 8a; light pink) for the Velkerri Formation (Kendall et al., 2009). On the other hand, the population of single-spot ages from shales deeper than 900 m instead agree with the age for the Derim Derim Dolerite (Fig. 8a; dark pink) intrusion ca. 1330–1300 Ma (Bodorkos et al., 2022; Yang et al., 2020; Nixon et al., 2021; Ahmad and Munson, 2013).

Importantly, these sample sets are statistically different from each other. This is graphically shown by their cumulative age distribution (CAD, Fig. 8b) and multidimensional scaling (MDS, Fig. 8c) plots. The second of these techniques statistically measures the dissimilarity between different age distributions through the Kolmogorov–Smirnov test (Vermeesch, 2013). In short, similar age distributions will plot closely to each other, whilst distributions that are increasingly dissimilar will plot further away (Vermeesch, 2013, 2012). Figure 8b and c show that samples shallower than 900 m had age distributions that are similar to each other (Fig. 8). Overall, these ages are statistically similar to the Re–Os constraint of the Velkerri Formation (Kendall et al., 2009), suggesting that they likely represent an early diagenetic age or burial age soon after deposition. On the other hand, the single-age distributions of samples deeper than 900 m are statistically different to the previous sample set. They form their own cluster, which in turn coincides with the age of the Derim Derim Dolerites (Bodorkos et al., 2022; Yang et al., 2020; Nixon et al., 2021; Ahmad and Munson, 2013). Consequently, the Rb–Sr shale ages from this section are unlikely to date the deposition of the Velkerri Formation, but they instead reflect a late-stage hydrothermal resetting induced by the intrusion.

The petrographic characteristics of assemblages in these samples are further evidence that the shales in the Velkerri Formation recorded two distinct thermochronological events. The abundant clays in samples from depths of 415, 520, and 696 m are predominantly illite, with trace amounts of chlorite, kaolinite, and montmorillonite (Table 1). However, they do not show typical irregular, angular detrital morphologies (Figs. 5, S2a–c). Instead, clay minerals in these samples form a matrix cement, filling in porous spaces and wrapping around detrital grains, suggesting that they formed within the sediment during burial diagenesis (Rafiei and Kennedy, 2019; Rafiei et al., 2020; Subarkah et al., 2021). Primary sedimentary structures with a similar compaction of clays along the bedding plane can also still be identified in these samples (Figs. 5, S2a–c, and Supplement). These petrographic relationships are further discussed in the Supplement and were similarly found in Roper Group shales elsewhere, indicating an early diagenetic origin (Subarkah et al., 2021; Rafiei and Kennedy, 2019). Moreover, the ages from these samples are all in agreement with the deposition of the Velkerri Formation dated at 1417 ± 29 Ma by Re–Os geochronology (Kendall et al., 2009), suggesting that the majority of illite formed relatively soon after sediment deposition.

Nevertheless, we also sought to identify any potential secondary alteration of these shales by analysing their geochemical signatures. Sm / Nd ratios are common geochemical proxies for screening alteration in shales because Nd is preferentially lost relative to Sm during post-depositional processes (Awwiller and Mack, 1989, 1991). In addition, fluid–rock reactions also have a significant impact on rare-earth element and yttrium solubility and transportation during hydrothermal events (Williams-Jones et al., 2012; Lev et al., 1999). Therefore, these parameters can be an effective tool for highlighting fingerprints of post-depositional geochemical mobilization (Fig. 7).

Samples from depths shallower than 900 m show no significant relationships between their total REEY concentrations and Sm / Nd ratios collected by laser ablation analysis or through traditional bulk trace element geochemistry (Cox et al., 2016). These support an interpretation that these ages form a minimum depositional age for the unit, recording an early diagenetic event as opposed to a late-stage secondary overprint. Furthermore, temperature constrains for the Velkerri Formation at depths 390–900 m suggest that they are well within the oil window (Figs. 3 and 4). As a result, we propose that this temperature window is not sufficient to disturb the Rb–Sr and trace element systems in these shales.

Conversely, shales collected from depths > 900 m showed petrographic evidence of post-depositional alteration (Figs. 5

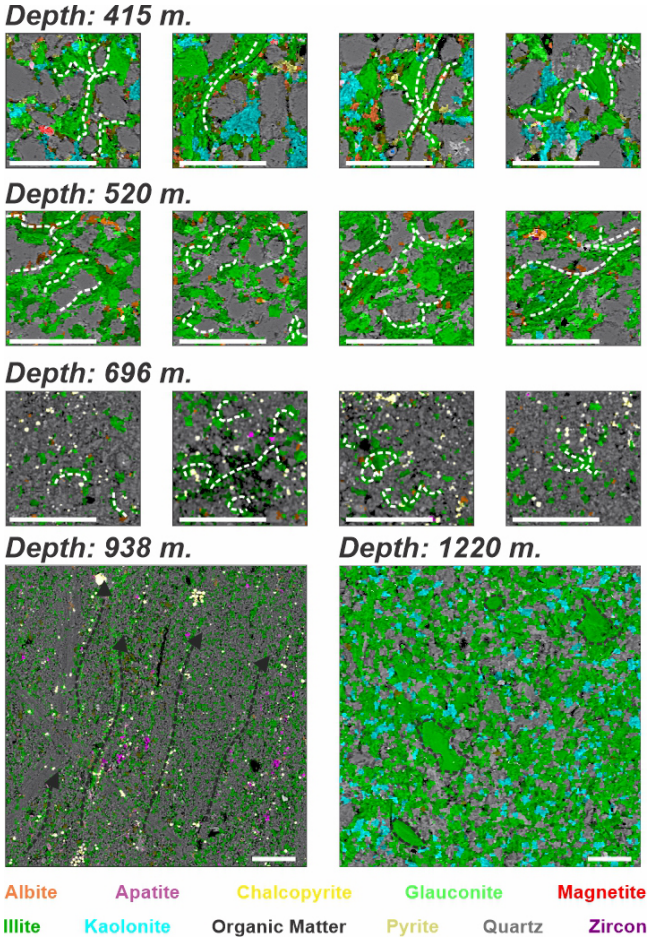

Figure 5. Spectral reflectance MLA maps of samples selected for in situ laser ablation analysis in this study overlain on top of their respective BSE images. Dashed white lines show illite assemblages wrapping around detrital grains and forming cements. Dashed black arrows show foliation in illite crystals. Dashed black lines show large illite crystals replacing previous clay assemblages. Solid white lines are 100 µm scale bars.

and S2d–e). Clay minerals the 938 m sample are fissile and foliated (Fig. 5). In addition, pyrite and apatite can be observed overgrowing illite and chlorite. Moreover, illite grains from the Kalala Member shale at 1220 m depth are notably larger and crystalline (Figs. 5 and S2d–e), with features inconsistent with an early diagenetic origin (Fig. S2d–e). Clay minerals were also found interlocking with quartz overgrowth and appear to replace earlier assemblages (Figs. 5 and S2d–e).

In addition to petrographic and geochronological disparities, samples from depths below 900 m display statistically significant relationships between total REEY concentrations and Sm / Nd ratios (Fig. 7). The shale chip analysed from 938 m had a positive relationship between an increase in Sm / Nd ratio and total REEY concentration (Pearson r: 0.580; R^2: 0.336), while the sample collected from depth 1220 m preserved a negative relationship between Sm / Nd ratio and total REEY values (Pearson r: −0.545; R^2: 0.297). These associations are similarly reflected in the bulk trace element data collated from Cox et al. (2016). In the compiled data, shales from deeper than 900 m demonstrate a strong affinity between these controls (Pearson r: −0.559; R^2: 0.312). These alteration indicators are further evidence that the Kalala Member at depths below 900 m experienced a late-stage secondary heating event, as trace elements are more readily mobilized in hydrothermal reactions (Williams-Jones et al., 2012; Poitrasson et al., 1995; Condie, 1991; Lev et al., 1999; Awwiller and Mack, 1989, 1991).

Importantly, thermal indicators from this interval suggest that kerogen in these shales are thermally overmature (Figs. 3 and 4). Previous studies have shown that the source rocks in the Velkerri Formation became overmature only when affected by magmatic events (Crick et al., 1988; George and Ahmed, 2002). As such, it is plausible that the Derim Derim Dolerite intersected in this well has imposed a hydrothermal alteration footprint onto the surrounding sediments via conductive heat loss and/or heat transfer fluids. This magmatic pulse would have recrystallized the former mineral assemblages or induced a second mineralization of clays, mobilized trace elements, and heated the kerogen within the Kalala Member to overmaturity. Thermal indicators (Figs. 4 and 9) suggest that source rocks within this interval may have experienced palaeotemperatures of at least 150 °C (Dellisanti et al., 2010; Merriman and Frey, 1999; Hunt, 1995; Welte and Tissot, 1984). This is in good agreement with evidence from aqueous fluid inclusions in quartz veins within the Derim Derim Dolerite elsewhere, which have suggested that hydrocarbons from the Velkerri Formation migrated in the cooling sill at similar temperatures (Dutkiewicz et al., 2004). Importantly, such hydrothermal systems seem to be sufficient for disturbing the Rb–Sr isotopic system of these samples.

7 Modelled predictions of the geothermal aureole induced by the Derim Derim Dolerite

Resetting of Rb–Sr geochronology and overmaturation of hydrocarbons in the Kalala Member within the Altree 2 well implies the presence of a secondary hydrothermal aureole extending ca. 800 m away from the Derim Derim Dolerite sill, which is intersected at present-day depth 1696 m. One-dimensional thermal modelling for a sill thickness of 75 m in the Mesoproterozoic suggests temperatures exceeding the oil window over 120 °C (Tissot et al., 1974; Waples, 1980) only extended ca. 700 m from the intrusion (Fig. 9a).

Samples at present-day depths of 938 and 1220 m yield Rb–Sr ages corresponding to emplacement timing of the Derim Derim Dolerite (Nixon et al., 2021; Yang et al., 2020), which suggests that the intrusion caused the chronometer to reset or induced a second mineralization of clay phases. Predicted temperatures experienced by the shallowest reset sam-

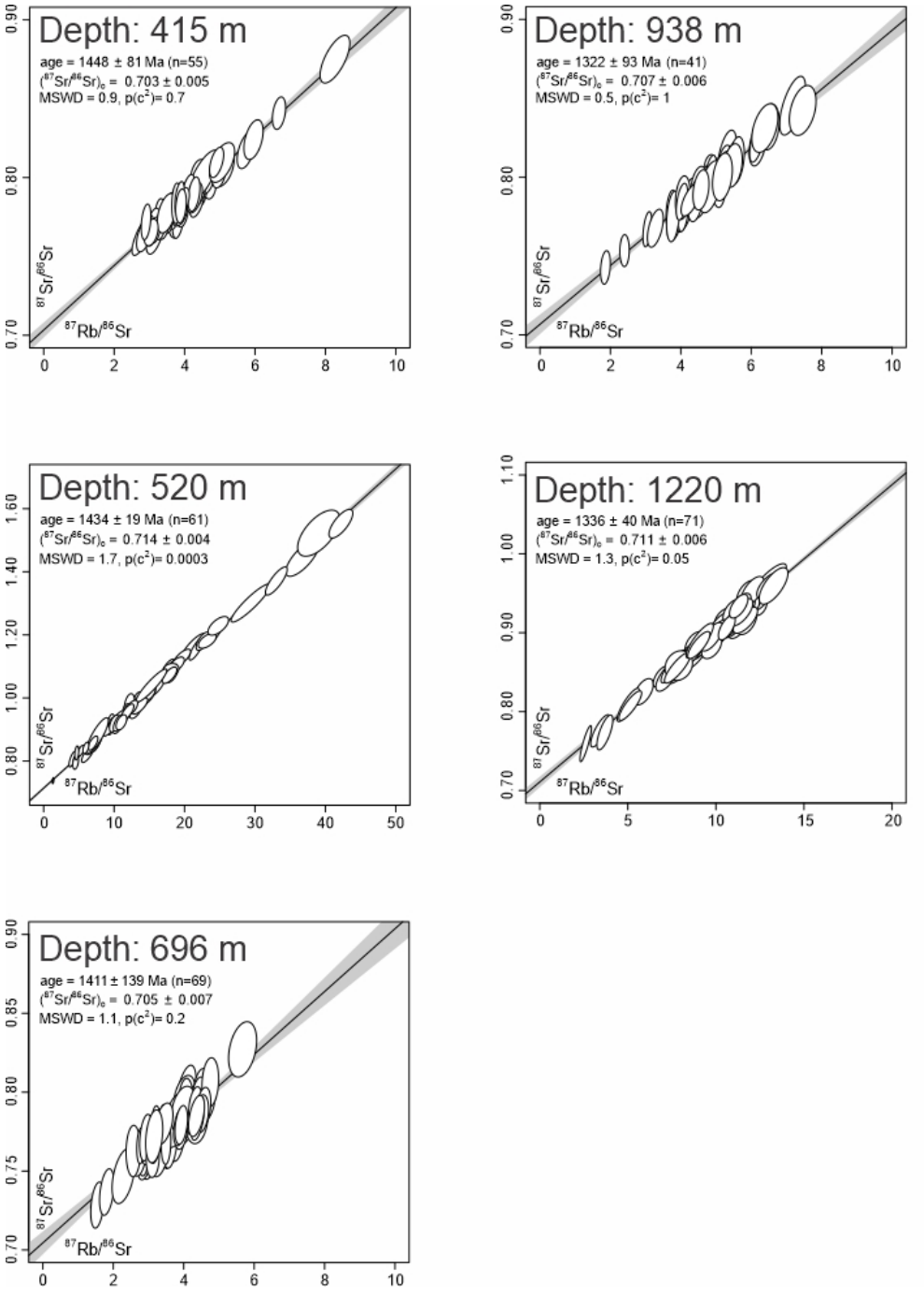

Figure 6. Summary of in situ Rb–Sr geochronological results from this study.

ple, however, are lower than the inferred closure temperatures for observed K–Ar and Rb–Sr in sheet silicates (Dodson, 1973; Tillberg et al., 2020; Torgersen et al., 2015; Yoder and Eugster, 1955). In a scenario in which a sill of thickness 75 m was intruded below samples, rocks from present-day depth of 938 m are only predicted to have experienced maximum heating to ca. 110 °C (Fig. 9c), with temperatures exceeding 100 °C for a duration of only ca. 150 ka (Fig. 9b).

Additionally, the eruption of lavas from the Kalkarindji LIP (Evins et al., 2009; Glass and Phillips, 2006; Jourdan et al., 2014) within the same vertical profile offer an intriguing opportunity to evaluate thermal resistance of the Rb–Sr system in shale-hosted clays in different conditions. Basaltic lavas of the ca. 510 Ma Cambrian Kalkarindji LIP (Evins et al., 2009; Glass and Phillips, 2006; Jourdan et al., 2014) are preserved above Proterozoic sedimentary rocks in

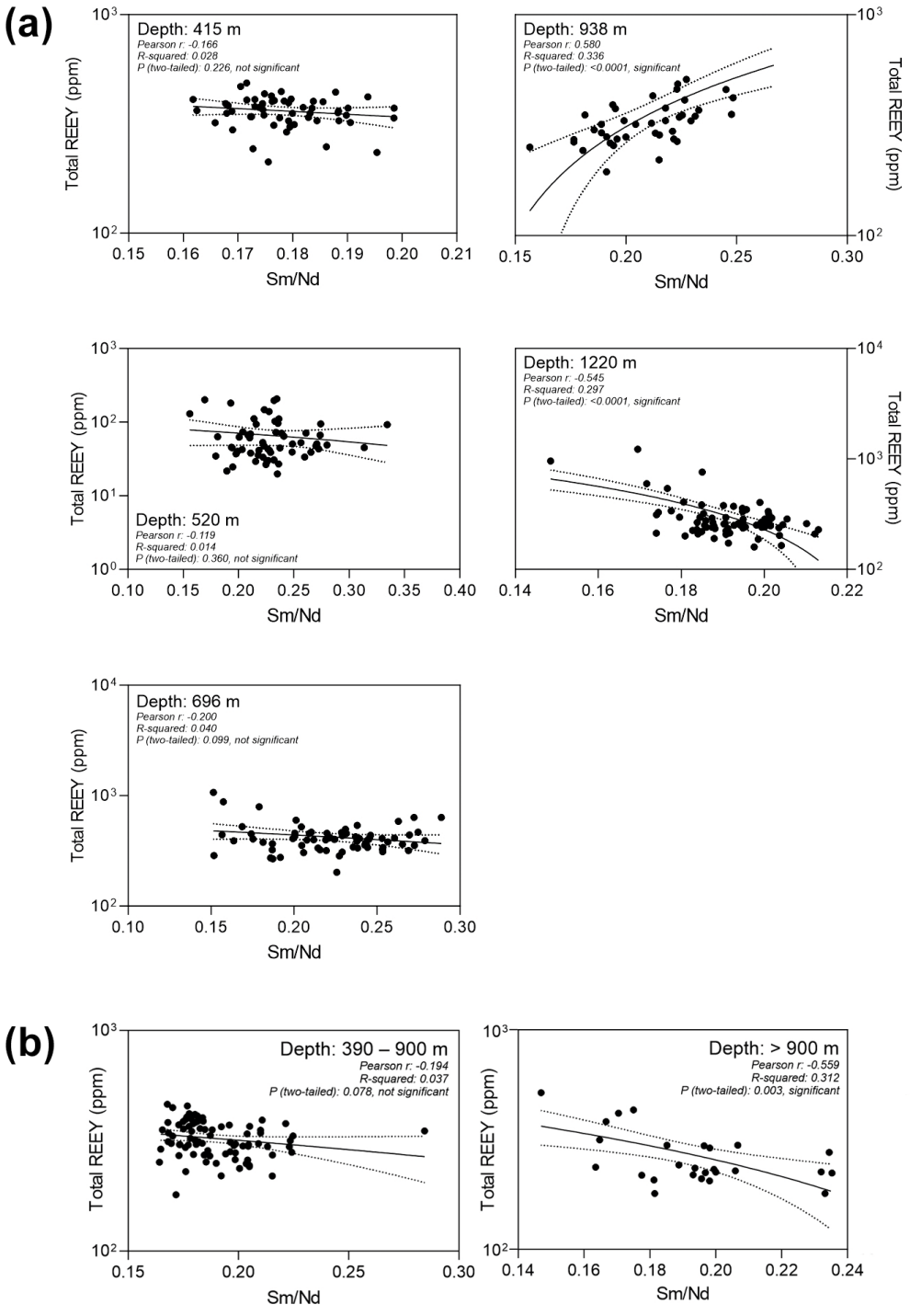

Figure 7. Statistical relationships between alteration proxies obtained from this study through laser ablation analysis **(a)** and whole-rock geochemical data **(b)** compiled from Cox et al. (2016).

the Altree 2 well. Furthermore, regional apatite fission track data suggest that the thermal pulses induced during this LIP extrusion were short-lived but sufficient (> 190 °C) to anneal tracks in the upper ∼ 500 m of the basin (Nixon et al., 2022). However, the shallowest samples taken in this study (at depths 415, 520, and 696 m) did not have their Rb–Sr isotopic system disturbed despite experiencing such temperatures from this reheating event. Consequently, the thermal profile for the sample at 415 m depth provides a minimum closure temperature constraint for short-lived conditions that

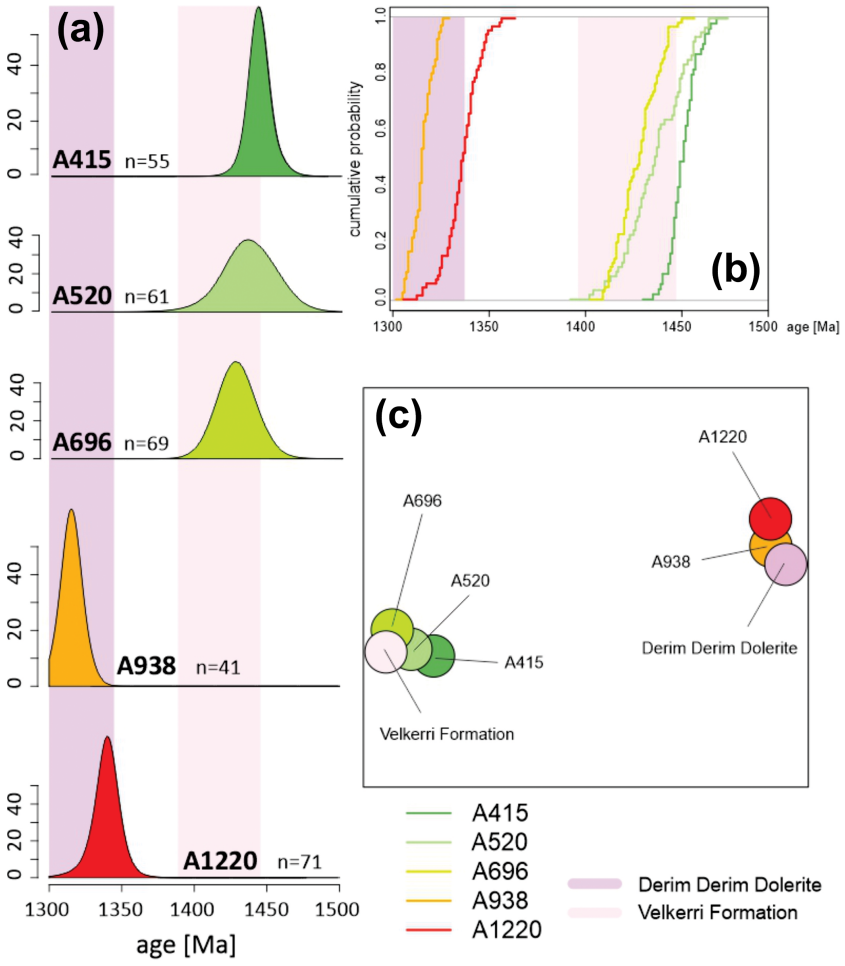

Figure 8. Single-spot ages from samples in this study illustrated by KDE **(a)**, CAD **(b)**, and MDS **(c)** plots. Note that the population of single-spot ages for samples at 415, 520, and 696 m depths all overlap with previous Velkerri Formation Re–Os age constraints shown in light pink (Kendall et al., 2009). On the other hand, samples at 938 and 1220 m depth are statistically different and instead agree with the Derim Derim Dolerite intrusion ca. 1330–1300 Ma (displayed in dark pink) (Bodorkos et al., 2022).

have not reset the Rb–Sr chronometer in these (presumably) dry shales over 800 million years after the Derim Derim Dolerite intrusion. Interestingly, the Cambrian palaeotemperatures imposed by the Kalkarindji lavas (Nixon et al., 2022) are notably higher (> 190 °C) than Mesoproterozoic palaeotemperatures reached by samples with Rb–Sr ages reset by the Derim Derim Dolerite (ca. 120 °C; Fig. 9a and b).

Such a disparity suggests that the presence of fluid (either connate or sourced from the intrusion), rather than just temperature, is likely to play a critical role in determining whether the Rb–Sr record in a shale is reset. As such, the geochemical system in shales within the aureole may be disturbed at lower temperatures, as trace and rare-earth elements are more easily mobilized in hydrothermal fluid systems (Villa, 1998; Nebel, 2014; Poitrasson et al., 1995; Williams-Jones et al., 2012; Li et al., 2019).

8 Conclusion

We show that the Velkerri Formation shales intersected by the Altree 2 well preserve evidence of an elevated Mesoproterozoic thermal gradient through an ∼ 800 m thick section away from the intrusion of a Derim Derim Dolerite sill (Figs. 3, 4, and 9). In situ Rb–Sr isotopic ages from the Wyworrie and Amungee members above this hydrothermal aureole yielded ages (Figs. 6 and 8) within error of their depositional age (Kendall et al., 2009). In addition, unaltered trace element compositions (Fig. 7) and petrographic relationships indicate that the shales preserve an early diagenetic origin (Fig. 5 and Supplement). However, the older Kalala Member that lies within the hydrothermal aureole yielded younger Rb–Sr ages (Figs. 6 and 8) consistent with the age of the Derim Derim Dolerite (Bodorkos et al., 2022; Ahmad and Munson, 2013; Nixon et al., 2021; Yang et al., 2020). Samples from this subset also recorded perturbed trace element

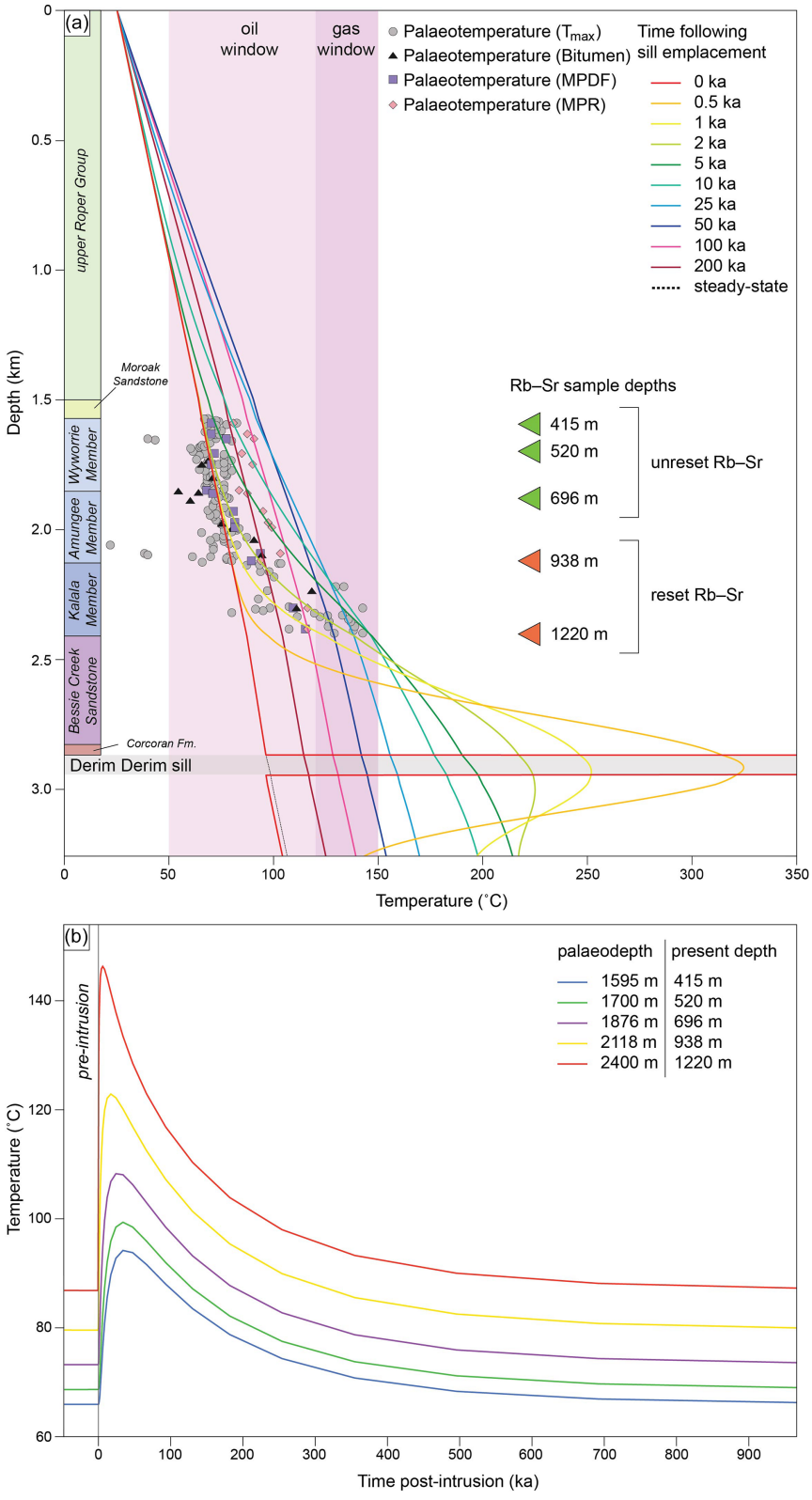

Figure 9. **(a)** One-dimensional thermal model for sill intrusion of 75 m thickness within the Altree 2 well depicting time steps following emplacement at 0 ka. Sill intrusion and Rb–Sr sample depths have been normalized to palaeodepths with 1.5 km of additional Mesoproterozoic sediments (Hall et al., 2021). Median palaeotemperature estimates from VR_{CALC} data from the Altree 2 well have been included for comparison to modelled temperatures. **(b)** Time–temperature profile for sample intervals within the Altree 2 well following intrusions of a sill of 75 m thick.

signatures (Fig. 7) and fissile, foliated, and crystalline illite morphologies (Fig. 5 and Supplement). This interval corresponds with disturbed thermal maturity indicators (Figs. 2, 3, and 4), suggesting that the Rb–Sr system is stable up to the maturation oil window and reset when the kerogen is overmature. Thermal modelling of the Derim Derim Dolerite suggests that a 75 m thick intrusion at the base of the Altree 2 well would have significantly elevated temperatures within 800 m of the sill, driving kerogen into the gas window, mobilizing trace elements and resetting the Rb–Sr isotopic system in the Kalala Member.

In conclusion, we show that the in situ Rb–Sr dating of the Velkerri Formation combined with common hydrocarbon maturity proxies can help reveal the thermochronological history of Proterozoic argillaceous rocks. When used in tandem, these methods can constrain the age of deposition and subsequent secondary, late-stage geological events. Importantly, we demonstrate that this technique can aid sedimentary-hosted resource exploration, as hydrothermal overprints can be identified and dated as previously demonstrated in Subarkah et al. (2021). Specifically, for hydrocarbon exploration, we show that the thermo-kinetic parameters of shale-hosted Rb–Sr isotopic system in hydrothermal settings can coincide with the maturation of kerogen into the gas window (Dodson, 1973; Espitalié, 1986; Kubler, 1967).

Code availability. Code to calculate error correlations on LADR can be accessed through https://github.com/jarredclloyd/PowerShell_LADR_errorcorrelation_workaround (last access: 25 August 2022, Lloyd, 2022).

Data availability. Data used in this study can be accessed through the Supplement. Additional figures can be found in https://doi.org/10.25909/6315ea488cc5f (Subarkah et al., 2022).

Supplement. The supplement related to this article is available online at: https://doi.org/10.5194/gchron-4-577-2022-supplement.

Author contributions. DS is responsible for the conceptualization, method development, data collection, and drafting of the paper. ALN is responsible for the conceptualization, computational modelling, and drafting of the paper. MJ is responsible for the conceptualization and drafting of the paper. ASC is responsible for primary supervision, project funding, and drafting of the paper. MLB is responsible for sampling, method development, experimentation, secondary supervision, and drafting of the paper. JF is responsible for method development, secondary supervision, and drafting of the paper. SEG is responsible for the method development and drafting of the paper. SH is responsible for conceptualization and drafting of the paper. AJ is responsible for the data collection and drafting of the paper.

Competing interests. The contact author has declared that none of the authors has any competing interests.

Disclaimer. Publisher's note: Copernicus Publications remains neutral with regard to jurisdictional claims in published maps and institutional affiliations.

Acknowledgements. This work was supported by the Australian Research Council Projects LP160101353 and LP200301457 with Santos Ltd, Empire Energy Group Ltd, Northern Territory Geological Survey, Teck Resources, BHP, and Origin as partners. The initial development and validation of in situ Rb-Sr dating technique at the University of Adelaide was also supported by Agilent Technologies Australia Ltd. This paper forms MinEx CRC contribution no. 2022/60. Aoife McFadden is thanked for their assistance in the MLA mapping of the samples in this study. Jarred Lloyd is thanked for his help in the laser data processing. Jarred Lloyd's code to process error correlations on LADR can be found at https://github.com/jarredclloyd/PowerShell_LADR_errorcorrelation_workaround (last access: 25 August 2022).

Financial support. This research has been supported by the Australian Research Council (grant nos. LP160101353 and LP200301457) and the MinEx CRC.

Review statement. This paper was edited by Daniela Rubatto and reviewed by two anonymous referees.

References

Abad, I. and Nieto, F.: Physical meaning and applications of the illite Kübler index: measuring reaction progress in low-grade metamorphism, Diagenesis and Low-Temperature Metamorphism, Theory, Methods and Regional Aspects, Seminarios, Sociedad Espanola: Sociedad Espanola Mineralogia, 53–64, https://citeseerx.ist.psu.edu/viewdoc/download?doi=10.1.1.556.7352&rep=rep1&type=pdf (last access: 25 August 2022), 2007.

Abbott, S. T. and Sweet, I. P.: Tectonic control on third-order sequences in a siliciclastic ramp-style basin: An example from the Roper Superbasin (Mesoproterozoic), northern Australia, Aust. J. Earth Sci., 47, 637–657, https://doi.org/10.1046/j.1440-0952.2000.00795.x, 2000.

Abbott, S. T., Sweet, I. P., Plumb, K. A., Young, D. N., Cutovinos, A., Ferenczi, P. A., and Pietsch, B. A.: Roper Region: Urapunga and Roper River Special, Northern Territory (Second Edition), 1 : 250 000 geological map series explanatory notes, SD 53-10, 11, Northern Territory Geological Survey and Geoscience Australia, Darwin, https://geoscience.nt.gov.au/gemis/ntgsjspui/handle/1/81859 (last access: 25 August 2022), 2001.

Ahmad, A. and Munson, T. J.: Geology and mineral resources of the Northern Territory, Special Publication, edited by: Munson, T. J., Johnston, K. J., and Fuller, M. H., Northern Territory Geolog-

ical Survey, https://geoscience.nt.gov.au/gemis/ntgsjspui/handle/1/81446 (last access: 25 August 2022), 2013.

Árkai, P., Sassi, F., and Desmons, J.: Towards a unified nomenclature in metamorphic petrology: 4, Very low-to low-grade metamorphic rocks. A proposal on behalf of the IUGS Subcommission on the Systematics of Metamorphic Rocks, International Union of Geological Sciences (IUGS), https://www.ugr.es/~agcasco/personal/IUGS/pdf-IUGS/scmr_low_r2_verylowtolowgrademetamorphicrocks.pdf (last access: 25 August 2022), 2002.

Armistead, S. E., Collins, A. S., Redaa, A., Jepson, G., Gillespie, J., Gilbert, S., Blades, M. L., Foden, J. D., and Razakamanana, T.: Structural evolution and medium-temperature thermochronology of central Madagascar: implications for Gondwana amalgamation, J. Geol. Soc. Aust., 177, 784, https://doi.org/10.1144/jgs2019-132, 2020.

Awwiller, D. N. and Mack, L. E.: Diagenetic Resetting of Sm-Nd Isotope Systematics in Wilcox Group Sandstones and Shales, San Marcos Arch, South-Central Texas, AAPG Bull., 39, 321–330, https://archives.datapages.com/data/gcags/data/039/039001/0321.htm (last access: 25 August 2022), 1989.

Awwiller, D. N. and Mack, L. E.: Diagenetic modification of Sm-Nd model ages in Tertiary sandstones and shales, Texas Gulf Coast, Geology, 19, 311–314, https://doi.org/10.1130/0091-7613(1991)019<0311:Dmosnm>2.3.Co;2, 1991.

Baldermann, A., Abdullayev, E., Taghiyeva, Y., Alasgarov, A., and Javad-Zada, Z.: Sediment petrography, mineralogy and geochemistry of the Miocene Islam Dağ Section (Eastern Azerbaijan): Implications for the evolution of sediment provenance, palaeo-environment and (post-) depositional alteration patterns, Sedimentology, 67, 152–172, 2020.

Bevan, D., Coath, C. D., Lewis, J., Schwieters, J., Lloyd, N., Craig, G., Wehrs, H., and Elliott, T.: In situ Rb–Sr dating by collision cell, multicollection inductively-coupled plasma mass-spectrometry with pre-cell mass-filter,(CC-MC-ICPMS/MS), J. Anal. Atom. Spectrom., 36, 917–931, 2021.

Blenkinsop, T. G.: Definition of low-grade metamorphic zones using illite crystallinity, J. Metamorph. Geol., 6, 623–636, 1988.

Bodorkos, S., Crowley, J. L., Claoué-Long, J. C., Anderson, J. R., and Magee, C. W.: Precise U–Pb baddeleyite dating of the Derim Derim Dolerite, McArthur Basin, Northern Territory: old and new SHRIMP and ID-TIMS constraints, Aust. J. Earth Sci., 68, 1–15, https://doi.org/10.1080/08120099.2020.1749929, 2022.

Boreham, C., Crick, I., and Powell, T.: Alternative calibration of the Methylphenanthrene Index against vitrinite reflectance: Application to maturity measurements on oils and sediments, Org. Geochem., 12, 289–294, 1988.

Brown, D. A., Simpson, A., Hand, M., Morrissey, L. J., Gilbert, S., Tamblyn, R., and Glorie, S.: Laser-ablation Lu-Hf dating reveals Laurentian garnet in subducted rocks from southern Australia, Geology, 50, 837–842, https://doi.org/10.1130/G49784.1, 2022.

Burtner, R. L. and Warner, M. A.: Relationship between illite/smectite diagenesis and hydrocarbon generation in Lower Cretaceous Mowry and Skull Creek shales of the northern Rocky Mountain area, Clay. Clay Miner., 34, 390–402, 1986.

Capogreco, N.: Provenance and thermal history of the Beetaloo Basin using illite crystallinity and zircon geochronology and trace element data, BSc thesis, University of Adelaide, https://hdl.handle.net/2440/126541 (last access: 25 August 2022), 2017.

Carvajal-Ortiz, H. and Gentzis, T.: Critical considerations when assessing hydrocarbon plays using Rock-Eval pyrolysis and organic petrology data: Data quality revisited, Int. J. Coal Geol., 152, 113–122, 2015.

Chamley, H.: Clay formation through weathering, in: Clay sedimentology, Springer, 21–50, https://doi.org/10.1007/978-3-642-85916-8_2, 1989.

Charbit, S., Guillou, H., and Turpin, L.: Cross calibration of K–Ar standard minerals using an unspiked Ar measurement technique, Chem. Geol., 150, 147–159, 1998.

Charlier, B. L., Ginibre, C., Morgan, D., Nowell, G. M., Pearson, D., Davidson, J. P., and Ottley, C.: Methods for the microsampling and high-precision analysis of strontium and rubidium isotopes at single crystal scale for petrological and geochronological applications, Chem. Geol., 232, 114–133, 2006.

Chen, J., Blume, H.-P., and Beyer, L.: Weathering of rocks induced by lichen colonization – a review, Catena, 39, 121–146, 2000.

Condie, K. C.: Another look at rare earth elements in shales, Geochim. Cosmochim. Ac., 55, 2527–2531, https://doi.org/10.1016/0016-7037(91)90370-K, 1991.

Cornford, C., Gardner, P., and Burgess, C.: Geochemical truths in large data sets. I: Geochemical screening data, Org. Geochem., 29, 519–530, 1998.

Cox, G. M., Jarrett, A., Edwards, D., Crockford, P. W., Halverson, G. P., Collins, A. S., Poirier, A., and Li, Z.-X.: Basin redox and primary productivity within the Mesoproterozoic Roper Seaway, Chem. Geol., 440, 101–114, https://doi.org/10.1016/j.chemgeo.2016.06.025, 2016.

Cox, G. M., Sansjofre, P., Blades, M. L., Farkas, J., and Collins, A. S.: Dynamic interaction between basin redox and the biogeochemical nitrogen cycle in an unconventional Proterozoic petroleum system, Sci. Rep., 9, 5200, https://doi.org/10.1038/s41598-019-40783-4, 2019.

Cox, G. M., Collins, A. S., Jarrett, A. J., Blades, M. L., Shannon, A. V., Yang, B., Farkas, J., Hall, P. A., O'Hara, B., and Close, D., and Baruch, E. T.: A very unconventional hydrocarbon play: the Mesoproterozoic Velkerri Formation of northern Australia, AAPG Bulletin, 106, 1213–1237, https://doi.org/10.1306/12162120148, 2022.

Crick, I., Boreham, C., Cook, A., and Powell, T.: Petroleum geology and geochemistry of Middle Proterozoic McArthur Basin, northern Australia II: Assessment of source rock potential, AAPG Bull., 72, 1495–1514, 1988.

Cuadros, J.: Clay minerals interaction with microorganisms: a review, Clay Miner., 52, 235–261, 2017.

Deepak, A., Löhr, S., Abbott, A. N., Han, S., Wheeler, C., and Sharma, M.: Testing the Precambrian reverse weathering hypothesis using a 1-billion-year record of marine shales, 2022 Goldschmidt Conference, 12 July 2022, Honolulu, Hawai'i, USA, https://conf.goldschmidt.info/goldschmidt/2022/meetingapp.cgi/Paper/10825 (last access: 25 August 2022), 2022.

Dellisanti, F., Pini, G. A., and Baudin, F.: Use of T max as a thermal maturity indicator in orogenic successions and comparison with clay mineral evolution, Clay Miner., 45, 115–130, 2010.

Dembicki Jr., H.: Three common source rock evaluation errors made by geologists during prospect or play appraisals, AAPG Bull., 93, 341–356, 2009.

Derkowski, A., Środoń, J., Franus, W., Uhlík, P., Banaś, M., Zieliński, G., Čaplovičová, M., and Franus, M.: Partial dissolution of glauconitic samples: Implications for the methodology of K-Ar and Rb-Sr dating, Clay. Clay Miner., 57, 531–554, https://doi.org/10.1346/CCMN.2009.0570503, 2009.

Dickin, A. P.: Radiogenic isotope geology, Cambridge university press, ISBN 9781107099449, 2018.

Disnar, J. R.: Détermination de paléotempératures maximales d'enfouissement de sédiments charbonneux à partir de données de pyrolyse, CR. Acad. Sci. II B, 303, 691–696, 1986.

Disnar, J. R.: Determination of maximum paleotemperatures of burial (MPTB) of sedimentary rocks from pyrolysis data on the associated organic matter: basic principles and practical application, Chem. Geol., 118, 289–299, https://doi.org/10.1016/0009-2541(94)90182-1, 1994.

Dodson, M. H.: Closure temperature in cooling geochronological and petrological systems, Contrib. Mineral. Petr., 40, 259–274, https://doi.org/10.1007/BF00373790, 1973.

Duddy, I., Green, P., Gibson, H., and Hegarty, K.: Regional Palaeothermal episodes in Northern Australia, Timor Sea Petrol. Geosci., Proc. Timor Sea Symp. 2003, 20 June 2003, Darwin, Australia, http://www.geotrack.com.au/papers/timor_sea_symposium_duddy_et_al.pdf (last access: 25 August 2022), 2004.

Dutkiewicz, A., Volk, H., Ridley, J., and George, S. C.: Geochemistry of oil in fluid inclusions in a middle Proterozoic igneous intrusion: implications for the source of hydrocarbons in crystalline rocks, Org. Geochem., 35, 937–957, https://doi.org/10.1016/j.orggeochem.2004.03.007, 2004.

Eberl, D., and Velde, B.: Beyond the Kubler index, Clay Miner., 24, 571–577, 1989.

Espitalié, J.: Use of Tmax as a maturation index for different types of organic matter: comparison with vitrinite reflectance, Collection colloques et séminaires – Institut français du pétrole, 475–496, http://pascal-francis.inist.fr/vibad/index.php?action=getRecordDetail&idt=7895690 (last access: 25 August 2022), 1986.

Espitalié, J., Madec, M., Tissot, B., Mennig, J., and Leplat, P.: Source rock characterization method for petroleum exploration, Offshore Technology Conference, 1 May 1977, Houston, Texas, USA, https://doi.org/10.4043/2935-MS, 1977.

Evins, L. Z., Jourdan, F., and Phillips, D. J. L.: The Cambrian Kalkarindji Large Igneous Province: Extent and characteristics based on new $^{40}Ar/^{39}Ar$ and geochemical data, Lithos, 110, 294–304, 2009.

Faure, G.: Principles of isotope geology, Wiley, https://www.osti.gov/biblio/7100564 (last access: 25 August 2022), 1977.

Field, D. and Råheim, A.: A geologically meaningless Rb–Sr total rock isochron, Nature, 282, 497–499, https://doi.org/10.1038/282497a0, 1979.

Merriman, R. J. and Frey, M.: Patterns of very low-grade metamorphism in metapelitic rocks, Low-grade Metamorphism, Blackwell, Oxford, 61–107, https://doi.org/10.1002/9781444313345.ch3, 1999.

Frogtech Geoscience: Digital Information Package, DIP: SEEBASE® study and GIS for greater McArthur Basin, Northern Territory Geological Survey, 17, https://geoscience.nt.gov.au/gemis/ntgsjspui/handle/1/87064 (last access: 25 August 2022), 2018.

Galán, E.: Genesis of clay minerals, Developments in clay science, 1, 1129–1162, 2006.

George, S. and Ahmed, M.: Use of aromatic compound distributions to evaluate organic maturity of the Proterozoic middle Velkerri Formation, McArthur Basin, Australia, https://archives.datapages.com/data/petroleum-exploration-society-of-australia/conferences/014/014001/pdfs/253.htm (last access: 25 August 2022), 2002.

Glass, L. M. and Phillips, D. J. G.: The Kalkarindji continental flood basalt province: A new Cambrian large igneous province in Australia with possible links to faunal extinctions, Geolog, 34, 461–464, 2006.

Gorojovsky, L. and Alard, O.: Optimisation of laser and mass spectrometer parameters for the in situ analysis of Rb / Sr ratios by LA-ICP-MS/MS, J. Anal. Atom. Spectrom., 35, 2322–2336, https://doi.org/10.1039/D0JA00308E, 2020.

Govindaraju, K., Rubeska, I., and Paukert, T.: 1994 Report On Zinnwaldite Zw-C Analysed By Ninety-Two Git-Iwg Member-Laboratories, Geostandard. Newslett., 18, 1–42, https://doi.org/10.1111/j.1751-908X.1994.tb00502.x, 1994.

Guggenheim, S., Bain, D. C., Bergaya, F., Brigatti, M. F., Drits, V. A., Eberl, D. D., Formoso, M. L., Galán, E., Merriman, R. J., and Peacor, D. R.: Report of the Association Internationale pour l'Etude des Argiles (AIPEA) Nomenclature Committee for 2001: order, disorder and crystallinity in phyllosilicates and the use of the "crystallinity index", Clay Miner., 37, 389–393, 2002.

Hahn, O. and Walling, E.: Über die Möglichkeit geologischer Altersbestimmungen rubidiumhaltiger Mineralien und Gesteine, Z. Anorg. Allg. Chem., 236, 78–82, 1938.

Hahn, O., Strassman, F., Mattauch, J., and Ewald, H.: Geologische Altersbestimmungen mit der strontiummethode, Chem. Ztg., 67, 55–56, 1943.

Hall, L., Boreham, C. J., Edwards, D. S., Palu, T., Buckler, T., Troup, A., and Hill, A.: Cooper Basin Source Rock Geochemistry, Geoscience Australia, https://doi.org/10.11636/Record.2016.006, 2016.

Hall, L. S., Orr, M. L., Lech, M. E., Lewis, S., Bailey, A. H. E., Owens, R., Bradshaw, B. E., and Bernardel, G.: Geological and Bioregional Assessments: assessing the prospectivity for tight, shale and deep-coal resources in the Cooper Basin, Beetaloo Subbasin and Isa Superbasin, The APPEA Journal, 61, 477–484, 2021.

Harrison, T. M., Heizler, M. T., McKeegan, K. D., and Schmitt, A. K.: In situ ^{40}K–^{40}Ca "double-plus" SIMS dating resolves Klokken feldspar ^{40}K–^{40}Ar paradox, Earth Planet. Sc. Lett., 299, 426–433, 2010.

Hillier, S.: Erosion, sedimentation and sedimentary origin of clays, in: Origin and mineralogy of clays, Springer, 162–219, https://doi.org/10.1007/978-3-662-12648-6_4, 1995.

Hogmalm, K. J., Zack, T., Karlsson, A. K. O., Sjöqvist, A. S. L., and Garbe-Schönberg, D.: In situ Rb–Sr and K–Ca dating by LA-ICP-MS/MS: an evaluation of N2O and SF6 as reaction gases, J. Anal. Atom. Spectrom., 32, 305-313, https://doi.org/10.1039/c6ja00362a, 2017.

Hogmalm, K. J., Dahlgren, I., Fridolfsson, I., and Zack, T.: First in situ Re-Os dating of molybdenite by LA-ICP-MS/MS, Miner. Deposita, 54, 821–828, 2019.

Hunt, J. M.: Petroleum geochemistry and geology, W. H. Freeman, ISBN 9780716724414, https://hero.epa.gov/hero/index.

cfm/reference/details/reference_id/8737015 (last access: 25 August 2022), 1995.

Isson, T. T. and Planavsky, N. J.: Reverse weathering as a long-term stabilizer of marine pH and planetary climate, Nature, 560, 471–475, https://doi.org/10.1038/s41586-018-0408-4, 2018.

Iyer, K., Svensen, H., and Schmid, D. W.: SILLi 1.0: a 1-D numerical tool quantifying the thermal effects of sill intrusions, Geosci. Model Dev., 11, 43–60, https://doi.org/10.5194/gmd-11-43-2018, 2018.

Jackson, M., Sweet, I., Page, R., and Bradshaw, B.: The South Nicholson and Roper Groups: evidence for the early Mesoproterozoic Roper Superbasin, Integrated Basin Analysis of the Isa Superbasin using Seismic, Well-log, and Geopotential Data: An Evaluation of the Economic Potential of the Northern Lawn Hill Platform: Canberra, Australia, Australian Geological Survey Organisation Record, 19 pp., 1999.

Jackson, M. J., Muir, M. D., and Plumb, K. A.: Geology of the Southern McArthur Basin, Northern Territory, Australian Government Pub. Service, https://dev.ecat.ga.gov.au/geonetwork/srv/api/records/a05f7892-9cf6-7506-e044-00144fdd4fa6 (last access: 25 August 2022), 1987.

Jarrett, A. J., Cox, G. M., Brocks, J. J., Grosjean, E., Boreham, C. J., and Edwards, D. S.: Microbial assemblage and palaeoenvironmental reconstruction of the 1.38 Ga Velkerri Formation, McArthur Basin, northern Australia, Geobiology, 17, 360–380, 2019.

Jarvie, D. M.: Factors affecting Rock-Eval derived kinetic parameters, Chem. Geol., 93, 79–99, 1991.

Jarvie, D. M., Claxton, B. L., Henk, F., and Breyer, J. T.: Oil and shale gas from the Barnett Shale, Ft, Worth Basin, Texas (abs.): AAPG Annual Meeting Program, 3 June 2001, Denver, Colorado, USA, A100, https://www.searchanddiscovery.com/abstracts/html/2001/annual/abstracts/0386.htm (last access: 25 August 2022), 2001.

Jenkin, G. R., Rogers, G., Fallick, A. E., and Farrow, C. M.: Rb-Sr closure temperatures in bi-mineralic rocks: a mode effect and test for different diffusion models, Chem. Geol., 122, 227–240, 1995.

Jochum, K. and Stoll, B.: Reference materials for elemental and isotopic analyses by LA-(MC)-ICP-MS: Successes and outstanding needs, in: Laser ablation ICP-MS in the Earth sciences: Current practices and outstanding issues, edited by: Sylvestor, P., Economic Geology, ISBN 9-0-921294-49-8, 40, 147–168, http://hdl.handle.net/11858/00-001M-0000-0014-8633-5 (last access: 25 August 2022), 2008.

Jochum, K. P., Willbold, M., Raczek, I., Stoll, B., and Herwig, K.: Chemical Characterisation of the USGS Reference Glasses GSA-1G, GSC-1G, GSD-1G, GSE-1G, BCR-2G, BHVO-2G and BIR-1G Using EPMA, ID-TIMS, ID-ICP-MS and LA-ICP-MS, Geostand. Geoanal. Res., 29, 285–302, 2005.

Jochum, K. P., Weis, U., Stoll, B., Kuzmin, D., Yang, Q., Raczek, I., Jacob, D. E., Stracke, A., Birbaum, K., Frick, D. A., Günther, D., and Enzweiler, J.: Determination of Reference Values for NIST SRM 610–617 Glasses Following ISO Guidelines, Geostand. Geoanal. Res., 35, 397–429, https://doi.org/10.1111/j.1751-908X.2011.00120.x, 2011.

Jourdan, F., Hodges, K., Sell, B., Schaltegger, U., Wingate, M., Evins, L., Söderlund, U., Haines, P., Phillips, D., and Blenkinsop, T. J. G.: High-precision dating of the Kalkarindji large igneous province, Australia, and synchrony with the Early–Middle Cambrian (Stage 4–5) extinction, Geology, 42, 543–546, 2014.

Kendall, B., Creaser, R., Gordon, G., and Anbar, A.: Re-Os and Mo isotope systematics of black shales from the Middle Proterozoic Velkerri and Wollogorang Formations, McArthur Basin, northern Australia, Geochim. Cosmochim. Ac., 73, 2534–2558, https://doi.org/10.1016/j.gca.2009.02.013, 2009.

Kennedy, M., Droser, M., Mayer, L. M., Pevear, D., and Mrofka, D.: Late Precambrian oxygenation; inception of the clay mineral factory, Science, 311, 1446–1449, 2006.

Kosakowski, G., Kunert, V., Clauser, C., Franke, W., and Neugebauer, H. J.: Hydrothermal transients in Variscan crust: paleotemperature mapping and hydrothermal models, Tectonophysics, 306, 325–344, https://doi.org/10.1016/S0040-1951(99)00064-5, 1999.

Kubler, B.: La cristallinité de l'illite et les zones tout à fait supérieures du métamorphisme, Etages tectoniques, 105–121, http://refhub.elsevier.com/S0048-9697(14)00679-2/rf0220 (last access: 25 August 2022), 1967.

Kvalheim, O. M., Christy, A. A., Telnæs, N., and Bjørseth, A.: Maturity determination of organic matter in coals using the methylphenanthrene distribution, Geochim. Cosmochim. Ac., 51, 1883–1888, https://doi.org/10.1016/0016-7037(87)90179-7, 1987.

Lanigan, K. and Ledlie, I. M.: Walton-1,2 EP 24 McArthur Basin, Northern Territory Well Completion Report, Pacific Oil and Gas, Northern Territory, AustraliaPR1989-0088, 1990.

Lanigan, K. and Torkington, J.: Well Completion Report EP19 – Sever 1, Daly Sub-basin of the McArthur Basin, Pacific Oil and Gas, Northern Territory, AustraliaPR1990-0069, 1991.

Laureijs, C. T., Coogan, L. A., and Spence, J.: In-situ RbSr dating of celadonite from altered upper oceanic crust using laser ablation ICP-MS/MS, Chem. Geol., 579, 120339, https://doi.org/10.1016/j.chemgeo.2021.120339, 2021.

Ledlie, I. M. and Maim, K.: Lawrence 1 EP 5 McArthur Basin, Northern Territory Well Completion Report, Pacific Oil and Gas, Northern Territory, AustraliaPR1989-0005, 1989.

Lee, M. and Parsons, I.: Biomechanical and biochemical weathering of lichen-encrusted granite: textural controls on organic–mineral interactions and deposition of silica-rich layers, Chem. Geol., 161, 385–397, 1999.

Lemiux, Y.: Altree 2, Burdo 1, Chanin 1, Jamison 1, McManus 1, Shenandoah 1A, Walton 2, Balmain-1, Elliott-1 pyrolysis and tight rock analysis, Talisman Energy, Advanced Well Technologies, Northern Territory Geological Survey, Northern Territory, AustraliaCSR0192, 2011.

Lev, S. M., McLennan, S. M., and Hanson, G. N.: Mineralogic controls on REE mobility during black-shale diagenesis, J. Sediment. Res., 69, 1071–1082, https://doi.org/10.2110/jsr.69.1071, 1999.

Li, S., Wang, X.-C., Li, C.-F., Wilde, S. A., Zhang, Y., Golding, S. D., Liu, K., and Zhang, Y.: Direct Rubidium-Strontium Dating of Hydrocarbon Charge Using Small Authigenic Illitic Clay Aliquots from the Silurian Bituminous Sandstone in the Tarim Basin, NW China, Sci. Rep., 9, 1–13, 2019.

Li, S.-S., Santosh, M., Farkaš, J., Redaa, A., Ganguly, S., Kim, S. W., Zhang, C., Gilbert, S., and Zack, T.: Coupled U-Pb and Rb-Sr laser ablation geochronology trace Archean to Proterozoic crustal evolution in the Dharwar Craton, India, Precambrian Res.,

343, 105709, https://doi.org/10.1016/j.precamres.2020.105709, 2020.

Lloyd, J. C.: PowerShell LADR error correlation workaround, GitHub [code], https://github.com/jarredclloyd/PowerShell_LADR_errorcorrelation_workaround, last access: 25 August 2022.

Mackenzie, F. T. and Kump, L. R.: Reverse weathering, clay mineral formation, and oceanic element cycles, Science, 270, 586–586, 1995.

Mählmann, R. F., Bozkaya, Ö., Potel, S., Le Bayon, R., Šegvić, B., and Nieto, F.: The pioneer work of Bernard Kübler and Martin Frey in very low-grade metamorphic terranes: paleo-geothermal potential of variation in Kübler-Index/organic matter reflectance correlations. A review, Swiss J. Geosci., 105, 121–152, 2012.

McMahon, W. J. and Davies, N. S.: Evolution of alluvial mudrock forced by early land plants, Science, 359, 1022–1024, 2018.

Mergelov, N., Mueller, C. W., Prater, I., Shorkunov, I., Dolgikh, A., Zazovskaya, E., Shishkov, V., Krupskaya, V., Abrosimov, K., and Cherkinsky, A.: Alteration of rocks by endolithic organisms is one of the pathways for the beginning of soils on Earth, Sci. Rep., 8, 1–15, 2018.

Meunier, A., Velde, B., and Velde, B.: Illite: Origins, evolution and metamorphism, Springer Science & Business Media, ISBN 9783540204862, 2004.

Minster, J. F., Ricard, L. P., and Allègre, C. J.: ^{87}Rb-^{87}Sr chronology of enstatite meteorites, Earth Planet. Sc. Lett., 44, 420–440, https://doi.org/10.1016/0012-821X(79)90081-5, 1979.

Mukherjee, I. and Large, R. R.: Pyrite trace element chemistry of the Velkerri Formation, Roper Group, McArthur Basin: Evidence for atmospheric oxygenation during the Boring Billion, Precambrian Res., 281, 13–26, https://doi.org/10.1016/j.precamres.2016.05.003, 2016.

Munson, T.: Sedimentary Characterisation of the Wilton Package, Greater MacArthur Basin, Northern Territory, Northern Territory Geological Survey, https://geoscience.nt.gov.au/gemis/ntgsjspui/handle/1/83806 (last access: 25 August 2022), 2016.

Munson, T. and Revie, D.: Stratigraphic subdivision of the Velkerri Formation, Roper Group, McArthur Basin, Northern Territory, Northern Territory Geological Survey, Record 2018-006, https://geoscience.nt.gov.au/gemis/ntgsjspui/handle/1/87322 (last access: 25 August 2022), 2018.

Nebel, O.: Rb–Sr Dating, in: Encyclopedia of Scientific Dating Methods, edited by: Rink, W. J. and Thompson, J. W., Springer Dordrecht, 1–19, https://doi.org/10.1007/978-94-007-6326-5_116-1, 2014.

Nebel, O., Scherer, E. E., and Mezger, K.: Evaluation of the ^{87}Rb decay constant by age comparison against the U–Pb system, Earth Planet. Sc. Lett., 301, 1–8, https://doi.org/10.1016/j.epsl.2010.11.004, 2011.

Nguyen, K., Love, G. D., Zumberge, J. A., Kelly, A. E., Owens, J. D., Rohrssen, M. K., Bates, S. M., Cai, C., and Lyons, T. W.: Absence of biomarker evidence for early eukaryotic life from the Mesoproterozoic Roper Group: Searching across a marine redox gradient in mid-Proterozoic habitability, Geobiology, 17, 247–260, 2019.

Nixon, A. L., Glorie, S., Collins, A. S., Blades, M. L., Simpson, A., and Whelan, J. A.: Inter-cratonic geochronological and geochemical correlations of the Derim Derim–Galiwinku/Yanliao reconstructed Large Igneous Province across the North Australian and North China cratons, Gondwana Res., 103, 473–486, https://doi.org/10.1016/j.gr.2021.10.027, 2021.

Nixon, A. L., Glorie, S., Hasterok, D., Collins, A. S., Fernie, N., and Fraser, G.: Low-temperature thermal history of the McArthur Basin: Influence of the Cambrian Kalkarindji Large Igneous Province on hydrocarbon maturation, Basin Res., https://doi.org/10.1111/bre.12691, online first, 2022.

Norris, A. and Danyushevsky, L.: Towards Estimating the Complete Uncertainty Budget of Quantified Results Measured by LA-ICP-MS, Goldschmidt, Boston, MA, USA, https://goldschmidtabstracts.info/2018/1894.pdf (last access: 25 August 2022), 2018.

NTGS: Altree 1 and 2 EP 24 McArthur Basin, Northern Territory Well Completion Report, Pacific Oil and Gas, Northern Territory, Australia, https://geoscience.nt.gov.au/gemis/ntgsjspui/handle/1/79405 (last access: 25 August 2022), 1989.

NTGS: Core Sample Analysis. Total Organic Carbon, Programmed Pyrolysis Data. Altree 2, Balmain 1, Elliott 1, Jamison 1, in: Core Sampling Reports, Falcon Oil & Gas Weatherford Laboratories, Northern Territory, Australia, https://geoscience.nt.gov.au/gemis/ntgsjspui/handle/1/84880 (last access: 25 August 2022), 2009.

NTGS: EP24 Altree 2 Petrology and organic geochemistry, Eni Australia, Geotechnical Services, Falcon Oil & Gas, Northern Territory Geological Survey, Northern Territory, Australia, CSR0185, https://geoscience.nt.gov.au/gemis/ntgsjspui/handle/1/84887 (last access: 25 August 2022), 2010.

NTGS: Quantitative X-Ray Diffraction Analysis of 30 samples, edited by: Northern Territory Geological Survey, Core Sampling Reports, Northern Territory Geological Survey, Northern Territory, Australia, https://geoscience.nt.gov.au/gemis/ntgsjspui/handle/1/84920 (last access: 25 August 2022), 2012.

NTGS: Basic Well Completion Report, NT EP167, Tarlee S3, Pangaea Resources, Northern Territory, Australia, PR2015-0016, https://geoscience.nt.gov.au/gemis/ntgsjspui/handle/1/83524 (last access: 25 August 2022), 2014.

NTGS: Basic Well Completion Report NT EP167 Birdum Creek 1, Pangaea Resources, Northern Territory, Australia, PR2016-W006, https://geoscience.nt.gov.au/gemis/ntgsjspui/handle/1/86120 (last access: 25 August 2022), 2015.

NTGS: Basic Well Completion Report NT – EP167 Wyworrie 1, Pangaea Resources, Northern Territory, Australia, PR2016-W007, https://geoscience.nt.gov.au/gemis/ntgsjspui/handle/1/86440 (last access: 25 August 2022), 2016.

Ola, P. S., Aidi, A. K., and Bankole, O. M.: Clay mineral diagenesis and source rock assessment in the Bornu Basin, Nigeria: Implications for thermal maturity and source rock potential, Mar. Petrol. Geol., 89, 653–664, 2018.

Olierook, H. K. H., Rankenburg, K., Ulrich, S., Kirkland, C. L., Evans, N. J., Brown, S., McInnes, B. I. A., Prent, A., Gillespie, J., McDonald, B., and Darragh, M.: Resolving multiple geological events using in situ Rb–Sr geochronology: implications for metallogenesis at Tropicana, Western Australia, Geochronology, 2, 283–303, https://doi.org/10.5194/gchron-2-283-2020, 2020.

Page, R. W., Jackson, M. J., and Krassay, A. A.: Constraining sequence stratigraphy in north Australian basins: SHRIMP U–Pb zircon geochronology between Mt Isa and McArthur River, Aust. J. Earth Sci., 47, 431–459, https://doi.org/10.1046/j.1440-0952.2000.00797.x, 2000.

Papanastassiou, D. A. and Wasserburg, G. J.: RbSr ages from the ocean of storms, Earth Planet. Sc. Lett., 8, 269–278, https://doi.org/10.1016/0012-821X(70)90111-1, 1970.

Pearce, N. J., Perkins, W. T., Westgate, J. A., Gorton, M. P., Jackson, S. E., Neal, C. R., and Chenery, S. P.: A compilation of new and published major and trace element data for NIST SRM 610 and NIST SRM 612 glass reference materials, Geostandard. Newslett., 21, 115–144, 1997.

Peters, K. E.: Guidelines for evaluating petroleum source rock using programmed pyrolysis, AAPG Bull., 70, 318–329, 1986.

Peters, K. E. and Cassa, M. R.: Applied source rock geochemistry: Chapter 5: Part II. Essential elements, American Association of Petroleum Geologists, 93–120, https://archives.datapages.com/data/specpubs/methodo2/data/a077/a077/0001/0050/0093.htm (last access: 25 August 2022), 1994.

Piedad-Sánchez, N., Izart, A., Martıìnez, L., Suárez-Ruiz, I., Elie, M., and Menetrier, C.: Paleothermicity in the Central Asturian Coal Basin, North Spain, Int. J. Coal Geol., 58, 205–229, https://doi.org/10.1016/j.coal.2004.02.001, 2004.

Plumb, K. and Wellman, P.: McArthur Basin, Northern Territory: mapping of deep troughs using gravity and magnetic anomalies, BMR J. Aust. Geol. Geop., 10, 243–251, 1987.

Poitrasson, F., Pin, C., and Duthou, J.-L.: Hydrothermal remobilization of rare earth elements and its effect on Nd isotopes in rhyolite and granite, Earth Planet. Sc. Lett., 130, 1–11, https://doi.org/10.1016/0012-821X(94)00257-Y, 1995.

Pollastro, R. M.: Considerations and applications of the illite/smectite geothermometer in hydrocarbon-bearing rocks of Miocene to Mississippian age, Clay. Clay Miner., 41, p. 119, 1993.

Radke, M., Willsch, H., Leythaeuser, D., and Teichmüller, M.: Aromatic components of coal: relation of distribution pattern to rank, Geochim. Cosmochim. Ac., 46, 1831–1848, 1982.

Rafiei, M. and Kennedy, M.: Weathering in a world without terrestrial life recorded in the Mesoproterozoic Velkerri Formation, Nat. Commun., 10, 3448, https://doi.org/10.1038/s41467-019-11421-4, 2019.

Rafiei, M., Löhr, S., Baldermann, A., Webster, R., and Kong, C.: Quantitative petrographic differentiation of detrital vs diagenetic clay minerals in marine sedimentary sequences: Implications for the rise of biotic soils, Precambrian Res., 350, 105948, https://doi.org/10.1016/j.precamres.2020.105948, 2020.

Rawlings, D. J.: Stratigraphic resolution of a multiphase intracratonic basin system: the McArthur Basin, northern Australia, Aust. J. Earth Sci., 46, 703–723, https://doi.org/10.1046/j.1440-0952.1999.00739.x, 1999.

Redaa, A., Farkaš, J., Gilbert, S., Collins, A. S., Wade, B., Löhr, S., Zack, T., and Garbe-Schönberg, D.: Assessment of elemental fractionation and matrix effects during in situ Rb–Sr dating of phlogopite by LA-ICP-MS/MS: implications for the accuracy and precision of mineral ages, J. Anal. Atom. Spectrom., 36, 322–344, https://doi.org/10.1039/D0JA00299B, 2021a.

Redaa, A., Farkaš, J., Hassan, A., Collins, A. S., Gilbert, S., and Löhr, S. C.: Constraints from in-situ Rb-Sr dating on the timing of tectono-thermal events in the Umm Farwah shear zone and associated Cu-Au mineralisation in the Southern Arabian Shield, Saudi Arabia, J. Asian Earth Sci., 224, 105037, https://doi.org/10.1016/j.jseaes.2021.105037, 2021b.

Revie, D.: XRD analysis greater McArthur Basin. NTGS Core Sampling Reports, Northern Territory Geological Survey, Northern Territory, Australia, https://geoscience.nt.gov.au/gemis/ntgsjspui/handle/1/85053 (last access: 25 August 2022), 2014.

Revie, D.: Interpretive summary of integrated petroleum geochemistry of selected wells in the greater McArthur Basin, NT, Australia, Northern Territory Geological Survey, Weatherford Laboratories, Northern Territory, Australia, CSR0413, 2016.

Revie, D. and MacDonald, G.: Volumetric resource assessment of the lower Kyalla and middle Velkerri formations of the McArthur Basin, Annual Geoscience Exploration Seminar (AGES) Proceedings, 29 March 2017, Alice Springs, Northern Territory, Australia, 29, https://geoscience.nt.gov.au/gemis/ntgsjspui/handle/1/85107 (last access: 25 August 2022), 2017.

Revie, D., Normington, V., and Jarrett, A.: Shale resource data from the greater McArthur Basin, Northern Territory Geological Survey, 1445-5358, 2022.

Ribeiro, B. V., Finch, M. A., Cawood, P. A., Faleiros, F. M., Murphy, T. D., Simpson, A., Glorie, S., Tedeschi, M., Armit, R., and Barrote, V. R.: From microanalysis to supercontinents: Insights from the Rio Apa Terrane into the Mesoproterozoic SW Amazonian Craton evolution during Rodinia assembly, J. Metamorph. Geol., 40, 631–663, https://doi.org/10.1111/jmg.12641, 2021.

Riediger, C. L.: Solid bitumen reflectance and Rock-Eval Tmax as maturation indices: an example from the "Nordegg Member", Western Canada Sedimentary Basin, Int. J. Coal Geol., 22, 295–315, https://doi.org/10.1016/0166-5162(93)90031-5, 1993.

Rösel, D. and Zack, T.: LA-ICP-MS/MS Single-Spot Rb-Sr Dating, Geostand. Geoanal. Res., 46, 143–168, https://doi.org/10.1111/ggr.12414, 2022.

Sander, R., Pan, Z., Connell, L. D., Camilleri, M., Grigore, M., and Yang, Y.: Controls on methane sorption capacity of Mesoproterozoic gas shales from the Beetaloo Sub-basin, Australia and global shales, Int. J. Coal Geol., 199, 65–90, 2018.

Scheiblhofer, E., Moser, U., Löhr, S., Wilmsen, M., Farkaš, J., Gallhofer, D., Bäckström, A. M., Zack, T., and Baldermann, A.: Revisiting Glauconite Geochronology: Lessons Learned from In Situ Radiometric Dating of a Glauconite-Rich Cretaceous Shelfal Sequence, Minerals, 12, 818, https://doi.org/10.3390/min12070818, 2022.

Schmitz, M. D. and Schoene, B.: Derivation of isotope ratios, errors, and error correlations for U-Pb geochronology using 205Pb-235U-(233U)-spiked isotope dilution thermal ionization mass spectrometric data, Geochem. Geophy. Geosy., 8, Q08006, https://doi.org/10.1029/2006GC001492, 2007.

Selby, D.: U-Pb zircon geochronology of the Aptian/Albian boundary implies that the GL-O international glauconite standard is anomalously young, Cretaceous Res., 30, 1263–1267, https://doi.org/10.1016/j.cretres.2009.07.001, 2009.

Şengün, F., Bertrandsson Erlandsson, V., Hogmalm, J., and Zack, T.: In situ Rb-Sr dating of K-bearing minerals from the orogenic Akçaabat gold deposit in the Menderes Massif, Western Anatolia, Turkey, J. Asian Earth Sci., 185, 104048, https://doi.org/10.1016/j.jseaes.2019.104048, 2019.

Shepherd, T. J. and Darbyshire, D. P. F.: Fluid inclusion Rb–Sr isochrons for dating mineral deposits, Nature, 290, 578–579, https://doi.org/10.1038/290578a0, 1981.

Simmons, E. C.: rubidiumRubidium: Element and geochemistry, in: Geochemistry, Springer Netherlands, Dordrecht, 555–556, https://doi.org/10.1007/1-4020-4496-8_278, 1998.

Simpson, A., Gilbert, S., Tamblyn, R., Hand, M., Spandler, C., Gillespie, J., Nixon, A., and Glorie, S.: In-situ LuHf geochronology of garnet, apatite and xenotime by LA ICP MS/MS, Chem. Geol., 577, 120299, https://doi.org/10.1016/j.chemgeo.2021.120299, 2021.

Simpson, A., Glorie, S., Hand, M., Spandler, C., Gilbert, S., and Cave, B.: In situ Lu–Hf geochronology of calcite, Geochronology, 4, 353–372, https://doi.org/10.5194/gchron-4-353-2022, 2022.

Singer, A.: The paleoclimatic interpretation of clay minerals in soils and weathering profiles, Earth-Sci. Rev., 15, 303–326, 1980.

Southgate, P. N., Bradshaw, B. E., Domagala, J., Jackson, M. J., Idnurm, M., Krassay, A. A., Page, R. W., Sami, T. T., Scott, D. L., Lindsay, J. F., McConachie, B. A., and Tarlowski, C.: Chronostratigraphic basin framework for Palaeoproterozoic rocks (1730–1575 Ma) in northern Australia and implications for base-metal mineralisation, Aust. J. Earth Sci., 47, 461–483, https://doi.org/10.1046/j.1440-0952.2000.00787.x, 2000.

Subarkah, D., Blades, M. L., Collins, A. S., Farkaš, J., Gilbert, S., Löhr, S. C., Redaa, A., Cassidy, E., and Zack, T.: Unraveling the histories of Proterozoic shales through in situ Rb-Sr dating and trace element laser ablation analysis, Geology, 50, 66–70, https://doi.org/10.1130/G49187.1, 2021.

Subarkah, D., Nixon, A., Jimenez Lloreda, M., Collins, A., Blades, M., Farkas, J., Gilbert, S., Holford, S., and Jarrett, A.: GCHRON-2022-8_SuppFigures, The University of Adelaide [figure], https://doi.org/10.25909/6315ea488cc5f, 2022.

Summons, R. E., Taylor, D., and Boreham, C. J.: Geochemical Tools For Evaluating Petroleum Generation In Middle Proterozoic Sediments Of The Mcarthur Basin, Northern Territory, Australia, The APPEA Journal, 34, 692–706, 1994.

Tamblyn, R., Hand, M., Morrissey, L., Zack, T., Phillips, G., and Och, D.: Resubduction of lawsonite eclogite within a serpentinite-filled subduction channel, Contrib. Mineral. Petr., 175, 74, https://doi.org/10.1007/s00410-020-01712-1, 2020.

Tamblyn, R., Hand, M., Simpson, A., Gilbert, S., Wade, B., and Glorie, S.: In situ laser ablation Lu–Hf geochronology of garnet across the Western Gneiss Region: campaign-style dating of metamorphism, J. Geol. Soc., 179, 4, https://doi.org/10.1144/jgs2021-094, 2021.

Taylor, D., Kontorovich, A. E., Larichev, A. I., and Glikson, M.: Petroleum Source Rocks In The Roper Group Of The Mcarthur Basin: Source Characterisation And Maturity Determinations Using Physical And Chemical Methods, The APPEA Journal, 34, 279–296, 1994.

Tillberg, M., Drake, H., Zack, T., Kooijman, E., Whitehouse, M. J., and Åström, M. E.: In situ Rb-Sr dating of slickenfibres in deep crystalline basement faults, Sci. Rep., 10, 562, https://doi.org/10.1038/s41598-019-57262-5, 2020.

Tissot, B., Durand, B., Espitalie, J., and Combaz, A.: Influence of nature and diagenesis of organic matter in formation of petroleum, AAPG Bull., 58, 499–506, 1974.

Tissot, B., Pelet, R., and Ungerer, P.: Thermal history of sedimentary basins, maturation indices, and kinetics of oil and gas generation, AAPG Bull., 71, 1445–1466, 1987.

Torgersen, E., Viola, G., Zwingmann, H., and Harris, C.: Structural and temporal evolution of a reactivated brittle–ductile fault – Part II: Timing of fault initiation and reactivation by K–Ar dating of synkinematic illite/muscovite, Earth Planet. Sc. Lett., 410, 212–224, https://doi.org/10.1016/j.epsl.2014.09.051, 2015.

Varajao, A. and Meunier, A.: Particle morphological evolution during the conversion of I/S to illite in Lower Cretaceous shales from Sergipe-Alagoas Basin, Brazil, Clay. Clay Miner., 43, 14–28, 1995.

Velde, B. and Espitalié, J.: Comparison of kerogen maturation and illite/smectite somposition in diagnesis, J. Petrol. Geol., 12, 103–110, 1989.

Velde, B. and Vasseur, G.: Estimation of the diagenetic smectite to illite transformation in time-temperature space, Am. Mineral., 77, 967–976, 1992.

Vermeesch, P.: Quantitative geomorphology of the White Mountains (California) using detrital apatite fission track thermochronology, J. Geophys. Res.-Earth, 112, F03004, https://doi.org/10.1029/2006JF000671, 2007.

Vermeesch, P.: On the visualisation of detrital age distributions, Chem. Geol., 312–313, 190–194, https://doi.org/10.1016/j.chemgeo.2012.04.021, 2012.

Vermeesch, P.: Multi-sample comparison of detrital age distributions, Chem. Geol., 341, 140–146, https://doi.org/10.1016/j.chemgeo.2013.01.010, 2013.

Vermeesch, P.: IsoplotR : A free and open toolbox for geochronology, Geosci. Front., 9, 1479–1493, https://doi.org/10.1016/j.gsf.2018.04.001, 2018.

Villa, I. M.: Isotopic closure, Terra Nova, 10, 42–47, https://doi.org/10.1046/j.1365-3121.1998.00156.x, 1998.

Villa, I. M., De Bièvre, P., Holden, N., and Renne, P.: IUPAC-IUGS recommendation on the half life of ^{87}Rb, Geochim. Cosmochim. Ac., 164, 382–385, 2015.

Volk, H., George, S. C., Dutkiewicz, A., and Ridley, J.: Characterisation of fluid inclusion oil in a Mid-Proterozoic sandstone and dolerite (Roper Superbasin, Australia), Chem. Geol., 223, 109–135, https://doi.org/10.1016/j.chemgeo.2004.12.024, 2005.

Waliczek, M., Machowski, G., Poprawa, P., Świerczewska, A., and Więcław, D.: A novel VRo, Tmax, and S indices conversion formulae on data from the fold-and-thrust belt of the Western Outer Carpathians (Poland), Int. J. Coal Geol., 234, 103672, https://doi.org/10.1016/j.coal.2020.103672, 2021.

Wang, X.-C., Li, Z.-X., Li, X.-H., Li, J., Liu, Y., Long, W.-G., Zhou, J.-B., and Wang, F. J. J. O. P.: Temperature, pressure, and composition of the mantle source region of Late Cenozoic basalts in Hainan Island, SE Asia: a consequence of a young thermal mantle plume close to subduction zones?, J. Petrology, 53, 177–233, https://doi.org/10.1093/petrology/egr061, 2012.

Waples, D. W.: Time and temperature in petroleum formation: application of Lopatin's method to petroleum exploration, AAPG Bull., 64, 916–926, 1980.

Warr, L. and Mählmann, R. F.: Recommendations for Kübler index standardization, Clay Miner., 50, 283–286, 2015.

Warr, L. N. and Rice, A. H. N.: Interlaboratory standardization and calibration of day mineral crystallinity and crystallite size data, J. Metamorph. Geol., 12, 141–152, 1994.

Warren, J. K., George, S. C., Hamilton, P. J., and Tingate, P.: Proterozoic Source Rocks: Sedimentology and Organic Characteristics of the Velkerri Formation, Northern Territory, Australia1, AAPG Bull., 82, 442–463, https://doi.org/10.1306/1D9BC435-172D-11D7-8645000102C1865D, 1998.

Welte, D. and Tissot, P.: Petroleum formation and occurrence, Springer, ISBN 9783642878138, 1984.

Wilhelms, A., Teln, N., Steen, A., and Augustson, J.: A quantitative study of aromatic hydrocarbons in a natural maturity shale sequence – the 3-methylphenanthrene/retene ratio, a pragmatic maturity parameter, Org. Geochem., 29, 97–105, https://doi.org/10.1016/S0146-6380(98)00112-0, 1998.

Williams-Jones, A., Migdisov, A., and Samson, I.: Hydrothermal Mobilisation of the Rare Earth Elements – a Tale of "Ceria" and "Yttria", Elements, 8, 355–360, https://doi.org/10.2113/gselements.8.5.355, 2012.

Wilson, M. J.: The origin and formation of clay minerals in soils: past, present and future perspectives, Clay Miner., 34, 7–25, 1999.

Yang, B., Smith, T. M., Collins, A. S., Munson, T. J., Schoemaker, B., Nicholls, D., Cox, G., Farkas, J., and Glorie, S.: Spatial and temporal variation in detrital zircon age provenance of the hydrocarbon-bearing upper Roper Group, Beetaloo Sub-basin, Northern Territory, Australia, Precambrian Res., 304, 140–155, https://doi.org/10.1016/j.precamres.2017.10.025, 2018.

Yang, B., Collins, A., Blades, M., Capogreco, N., Payne, J., Munson, T., Cox, G., and Glorie, S.: Middle-late Mesoproterozoic tectonic geography of the North Australia Craton: U–Pb and Hf isotopes of detrital zircon grains in the Beetaloo Subbasin, Northern Territory, Australia, J. Geol. Soci., 176, 771, https://doi.org/10.1144/jgs2018-159, 2019.

Yang, B., Collins, A. S., Cox, G. M., Jarrett, A. J. M., Denyszyn, S., Blades, M. L., Farkaš, J., and Glorie, S.: Using Mesoproterozoic Sedimentary Geochemistry to Reconstruct Basin Tectonic Geography and Link Organic Carbon Productivity to Nutrient Flux from a Northern Australian Large Igneous Province, Basin Res., 32, 1734–1750, https://doi.org/10.1111/bre.12450, 2020.

Yang, S. and Horsfield, B.: Critical review of the uncertainty of Tmax in revealing the thermal maturity of organic matter in sedimentary rocks, Int. J. Coal Geol., 225, 103500, https://doi.org/10.1016/j.coal.2020.103500, 2020.

Yang, Y.-H., Zhang, H.-F., Chu, Z.-Y., Xie, L.-W., and Wu, F.-Y.: Combined chemical separation of Lu, Hf, Rb, Sr, Sm and Nd from a single rock digest and precise and accurate isotope determinations of Lu–Hf, Rb–Sr and Sm–Nd isotope systems using Multi-Collector ICP-MS and TIMS, Int. J. Mass Spectrom., 290, 120–126, 2010.

Yim, S.-G., Jung, M.-J., Jeong, Y.-J., Kim, Y., and Cheong, A. C.-s.: Mass fractionation of Rb and Sr isotopes during laser ablation-multicollector-ICPMS: in situ observation and correction, Journal of Analytical Science and Technology, 12, 10, https://doi.org/10.1186/s40543-021-00263-9, 2021.

Yoder, H. S. and Eugster, H. P.: Synthetic and natural muscovites, Geochim. Cosmochim. Ac., 8, 225–280, https://doi.org/10.1016/0016-7037(55)90001-6, 1955.

Zack, T., and Hogmalm, K. J.: Laser ablation Rb / Sr dating by online chemical separation of Rb and Sr in an oxygen-filled reaction cell, Chem. Geol., 437, 120–133, https://doi.org/10.1016/j.chemgeo.2016.05.027, 2016.

Zambell, C., Adams, J., Gorring, M., and Schwartzman, D.: Effect of lichen colonization on chemical weathering of hornblende granite as estimated by aqueous elemental flux, Chem. Geol., 291, 166–174, 2012.